HHS Public Access

Author manuscript

FASEB J. Author manuscript; available in PMC 2023 August 01.

Published in final edited form as:

FASEB J. 2022 August ; 36(8): e22428. doi:10.1096/fj.202200369R.

Glucose Uptake by GLUT1 in Photoreceptors is Essential for Outer Segment Renewal and Rod Photoreceptor Survival

Lauren L. Daniele[1,#], **John Y.S. Han**[1,#], **Ivy S. Samuels**[2,3,#], **Ravikiran Komirisetty**[1], **Nikhil Mehta**[1], **Jessica L. McCord**[1], **Minzhong Yu**[2,8], **Yekai Wang**[4,5], **Kathleen Boesze-Battaglia**[6], **Brent A. Bell**[7], **Jianhai Du**[4,5], **Neal S. Peachey**[2,3,8], **Nancy J. Philp**[1,*]

[1]Department of Pathology, Anatomy, and Cell Biology, Thomas Jefferson University, Philadelphia, PA

[2]Cole Eye Institute, Cleveland Clinic, Cleveland, OH

[3]Louis Stokes Cleveland VA Medical Center, Cleveland, OH

[4]Department of Ophthalmology and Visual Sciences, West Virginia University, Morgantown, WV

[5]Department of Biochemistry, West Virginia University, Morgantown, WV

[6]Department of Basic and Translational Sciences, Penn Dental Medicine, University of Pennsylvania, Philadelphia, PA

[7]Department of Ophthalmology, University of Pennsylvania, Philadelphia, PA

[8]Department of Ophthalmology, Cleveland Clinic Lerner College of Medicine of Case Western Reserve University, Cleveland, OH

Abstract

Photoreceptors consume glucose supplied by the choriocapillaris to support phototransduction and outer segment (OS) renewal. Reduced glucose supply underlies photoreceptor cell death in inherited retinal degeneration and age-related retinal disease. We have previously shown that restricting glucose transport into the outer retina by conditional deletion of *Slc2a1* encoding GLUT1 resulted in photoreceptor loss and impaired OS renewal. However, retinal neurons, glia, and the retinal pigment epithelium (RPE) play specialized, synergistic roles in metabolite supply and exchange, and the cell-specific map of glucose uptake and utilization in the retina is incomplete. In these studies, we conditionally deleted *Slc2a1* in a pan-retinal or rod-specific manner to better understand how glucose is utilized in the retina. Using non-invasive ocular imaging, electroretinography, histochemical and biochemical analyses we show that genetic deletion of *Slc2a1* from retinal neurons and Müller glia results in reduced OS growth and

*Corresponding Author: nancy.philp@jefferson.edu, Thomas Jefferson University 1020 Locust St. Philadelphia, PA 19107 Phone: 215 503-7854.

#Denotes equal contribution

Author Contributions

LLD, JYSH, ISS, all equally contributed to the writing of this manuscript. NJP conceived the project. NJP, NSP, ISS, JYSH, and LLD designed the experiments. ISS generated the *RetΔGlut1* mice. NSP generated the *RodΔGlut1* mice. NJP, LLD, JYSH, RK, NM and JLM performed, and analyzed all biochemical and molecular assays. JYSH analyzed RNAseq libraries. ISS and MY acquired and analyzed ERG data. YW and JD performed the LC MS/MS, acquired and analyzed the data. BAB and JYSH performed and acquired SD-OCT and cSLO. JYSH analyzed SD-OCT data. LLD analyzed cSLO data. NSP and KBB provided expertise in interpretation of ERG and metabolomics data.

progressive rod but not cone photoreceptor cell death. Rhodopsin levels were severely decreased even at postnatal day 20 when OS length was relatively normal. Arrestin levels were not changed suggesting that glucose uptake is required to synthesize membrane glycoproteins. Rod-specific deletion of *Slc2a1* resulted in similar changes in OS length and rod photoreceptor cell death. These studies demonstrate that glucose is an essential carbon source for rod photoreceptor cell OS maintenance and viability.

Introduction

As is the case in the brain, the main energy source for the neural retina is glucose, and a decrease in glucose availability in the outer retina has been implicated in photoreceptor death in retinitis pigmentosa (RP) as well as age-related macular degeneration (1-7). Therefore, unraveling how glucose and its metabolic derivatives support retinal health and function is essential to develop treatment strategies for retinal degenerative and age-related diseases.

Photoreceptor-specific genetic disruption of glycolytic enzymes in mice has been used to understand how aerobic glycolysis supports the metabolism and function of the mouse outer retina (4, 6, 8-12). In many cases, enzyme deletion only partially disrupts the pathway of interest due to compensation by alternate pathways and isozymes (6, 9). Additionally, enzymes may have non-enzymatic functions further complicating the interpretation of the phenotype (11, 13). In contrast, targeted deletion of solute transporters themselves can provide a clearer understanding of the role(s) played by a given metabolite, such as glucose, in supporting cellular metabolism (7, 14, 15).

It is well established that the retina consumes glucose for aerobic glycolysis, converting over 90% to lactate, to supply roughly half of the ATP produced (16-19). It is hypothesized that the majority of retinal aerobic glycolysis occurs in photoreceptors (20). However, when we restricted glucose transported to photoreceptors by knocking out the glucose transporter GLUT1, encoded by *Slc2a1*, in the retinal pigment epithelium (RPE) we did not find decreased levels of ATP in the neural retina, despite observing a decrease in levels of retinal lactate (7). While rod photoreceptors constitute 50% of the cells in the neural retina, rod-specific knockout of lactate transporters (14), or other enzymes required for aerobic glycolysis (HK2 and PKM2) (6, 9), resulted in only ~14-20% decrease in lactate efflux. Furthermore, mice with a conditional deletion of the mitochondrial pyruvate carrier (MPC) presented with reduced electroretinograms (ERGs) but more modest changes in photoreceptor cell number or outer segment (OS) length (4). These studies suggest that glycolysis, the pentose phosphate shunt, and oxidative metabolism combine to support the metabolic demands of photoreceptor cells.

The daily renewal of OSs is essential for maintaining visual function in photoreceptors and requires abundant synthesis and post-translational modification of opsin. It has been clearly demonstrated that glucose and glycolysis are required to sustain OS renewal (7, 21). Glucose and its glycolytic intermediates have been found to be important precursors for protein, nucleotide, and lipid synthesis (22), all of which are important for photoreceptor OS renewal. It was previously shown that glucose deprivation results in decreased G-protein

glycosylation (23), and that mutations of rhodopsin glycosylation sites resulted in decreased rhodopsin maturation and trafficking, shortening of OS length and photoreceptor cell death (24), suggesting glucose is required for the synthesis and maturation of opsin. To directly investigate how glucose is utilized in the retina, we generated and characterized mouse models lacking the glucose transporter GLUT1 in retinal neurons and Müller glia, or only in rod photoreceptors. We demonstrate that GLUT1 is the primary glucose transporter in the outer retina, and that glucose deprivation leads to a reduction in rod and cone opsins and shortened OS. These studies emphasize that in addition to the catabolic metabolism of glucose to produce ATP and lactate, glucose is required for anabolic metabolism in the photoreceptor cells to support OS renewal.

Materials and Methods

Animal Models

Mice carrying a floxed *Slc2a1* allele, a gift from E. Dale Abel (25; Jax stock #031871), were crossed to two different transgenic mouse lines to target the deletion of *Slc2a1* in a pan-retinal or rod-photoreceptor-specific manner. The generation of *Crx-Cre; Glut1*$^{flox/flox}$ mice (hereafter *RetΔGlut1*) has been described (26); control littermates were *Glut1*$^{flox/+}$*Cre* positive and *Glut1*$^{flox/flox}$ *Cre* negative mice. To generate a tamoxifen-inducible line lacking *Glut1* in rod photoreceptors (*Rod-Cre; Glut1*$^{flox/flox}$; hereafter *RodΔGlut1*), we crossed *Glut1*$^{flox/flox}$ mice with a transgenic line in which tamoxifen-inducible *Cre recombinase* has been knocked into the rod-specific *PDE6G* allele, a gift from Stephan Tsang (27). Tamoxifen (100 mg/ml in ethanol, diluted with corn oil to 10 mg/ml, administered by intraperitoneal injection at 100 μg/g body weight on 3 consecutive days beginning at 5 weeks of age) was also administered to control littermates (*Glut1*$^{flox/flox}$*; Cre negative*). All animals were kept under a 12:12 light-dark cycle. All animal procedures were conducted with the approval of the Institutional Animal Care & Use Committees of Thomas Jefferson University, the Louis Stokes Cleveland VA Medical Center, or the Cleveland Clinic, and conformed to the ARVO statement for use of animals in ophthalmic and vision research.

Single Cell RNAseq Analysis

scRNAseq libraries of neural retinas from 1 month old wild type animals (GSE153673) were downloaded (28). To begin, the experimental samples from methanol-fixed tissue and the NRL-GFP transgenic mouse line were excluded. The remaining four datasets (GSM4649092, GSM4649093, GSM4649095, and GSM4649096) were read into the R-studio (v2022.02.2 Build 485) using the Seurat package (29, 30) function "Read10X_h5". Following the Seurat vignettes for basic scRNAseq-seq integration and "sctransform", the data were combined and normalized. Cell types of each cluster were identified using known markers (31), and scores were given to each cell by the Seurat AddModuleScore function and averaged for all markers per cell type. Similar to a published pipeline for scRNAseq analysis of the retina (28), the maximum module score was identified, and compared to the second-highest cell type score. Cells were labeled if the maximum score was at least three times the second-highest score, unless the second highest score was zero, then an arbitrary value of 1 was needed. Ambiguously scored cells were removed. Expression values were transformed into transcript per million (TPM). Genes encoding for proteins with

glucose transmembrane transport activities (GO:5355) were selected for further analysis. TPM values were averaged per cell type and, after Log2 transformation, used to generate heatmaps using 'pheatmap' package. Endothelial cells were not included in the heatmap.

In situ hybridization

Tissue samples for *in situ* hybridization and other assays were obtained from mice euthanized by an overdose of ketamine (>100 mg/kg) and xylazine (>10 mg/kg) followed by cervical dislocation. Enucleated eyes were immediately embedded in Neg-50™ Frozen Section Medium (Cat# 6502, Thermo Scientific) and frozen in liquid nitrogen. Blocks were then cryosectioned (8 μm) and placed on positively charged Diamond white glass microscope slides (Cat#1358W, Globe Scientific, Paramus, NJ). RNAscope was performed on fresh frozen sections using probes for *Slc2a1* and *Slc2a3* with the Manual Red Detection Kit 2.5 (Advanced Cell Diagnostics, Hayward, CA) following manufacturer's instruction. Briefly, fresh frozen sections were fixed with ice cold 4% PFA for 15 minutes at 4°C and then dehydrated in ethanol. After a hydrophobic barrier was drawn around the entire slide using an ImmEdge Hydrophobic Barrier PAP Pen (Cat# H-400, Vector Laboratories, Burlingame, CA), the sections were pre-treated with hydrogen peroxide and Protease IV for 15 minutes. Slides were incubated with RNAscope probes for *Slc2a1* (GLUT1) (Mm-*Slc2a1*, Cat# 458671, Advanced Cell Diagnostic, Hayward, CA) or *Slc2a3* (GLUT3) (Mm-*Slc2a3*, Cat# 451571, Advanced Cell Diagnostic, Hayward, CA), for 2 hours at 40°C using HybEZ™ Hybridization System (Cat# 241000, Advanced Cell Diagnostic, Hayward, CA). Preamp steps 1-6 were performed and visualized using RNAscope 2.5 HD Manual Detection Kit Red (Cat# 322350, Advanced Cell Diagnostic, Hayward, CA). Preamp step 5 for *Slc2a1* was 20 minutes, and 30 minutes for *Slc2a3*. Samples were washed with PBS and stained with DAPI for 5 minutes. The sections were mounted using Gelvatol. The sections were imaged on Zeiss LSM780 NLO confocal microscope using the 20x objective.

Tissue preparation and immunofluorescence

Enucleated eyes were immediately placed into 4% paraformaldehyde (PFA) (Cat# 15710, Electron Microscopy Sciences, Hatfield, PA) for 2 minutes. The eyes were placed onto a dish in 1x PBS, and the cornea was removed. Eyecups were placed in 1 mL of 4% PFA at room temperature on a rocker. After 2 hours, the lens was removed, and the remaining eye cup was equilibrated in a stepwise manner with sucrose solutions that ranged in concentration from 5% to 30%. Globes were oriented within cryomolds in Neg-50™ Frozen Section Medium (Cat# 6502, Thermo Scientific) so that the superior/inferior axis was aligned with the sectioning plane (32). Cryosections (8 μm thick) were collected on positively charged Diamond white glass microscope slides (Cat#1358W, Globe Scientific, Paramus, NJ) and stored at −20°C.

For immunofluorescence confocal microscopy, frozen sections were brought to room temperature and a hydrophobic barrier was drawn around the samples on the slide using a Hydrophobic Barrier PAP Pen (Cat# H-400, Vector Laboratories, Burlingame, CA). 1x PBS was used to wash away the Neg-50™ Frozen Section Medium and sections were blocked in PBS with 5% BSA and 0.1% Tween 20 (PBST) for 1 hour at room temperature. Antibodies were diluted in PBST with 1% BSA and sections were incubated with the

primary antibodies overnight at 4°C. The slides were washed 3x with PBST then incubated with the appropriate Alexa Fluor 488 - or Alexa Fluor 555 - conjugated secondary antibodies diluted in PBST with 1% BSA for 30 minutes. See Table 1 for sources and dilutions of all primary and secondary antibodies used for immunofluorescence labeling. Slides were then washed 3x in PBST and 1x in PBS then incubated with DAPI for 10 minutes. Slides were washed 2x in PBS and coverslips were mounted with Gelvatol. For avidin labeling, slides were washed 3x in PBS with 0.1% Tween 20 then incubated with avidin conjugated to Alexa Fluor 488 (Cat# A21370, Thermo Fisher Scientific) for 1 hour at room temperature, followed by washes, DAPI counterstaining and mounting as above. All slides were imaged using a Zeiss LSM780 NLO confocal/multiphoton microscope.

Western Blot

Retinas were isolated from eyecups and protein was extracted using 100 µl per retina in Pierce@ RIPA buffer (Radioimmunoprecipitation Assay, Cat# 89900, Thermo Scientific, Rockford, IL) with Halt™ Protease Inhibitor (Cat# 78420, Thermo Scientific). Retinal samples were homogenized by trituration with a P200 pipette. Samples were placed on ice for 30 minutes with intermittent vortexing. The samples were centrifuged at 12,000 x RPM for 30 minutes, and the supernatants were removed for protein quantification by BCA Protein Assay Kit (Cat # 23225, Thermo Fisher Scientific). A total of 5, 2.5 or 0.25 µg of retina protein was loaded on 4-12% NuPage Bis-Tris Protein gels (Cat# NP0321BOX, Invitrogen). Gels were run for 50 minutes at 200V, per manufacturer's instructions. Gels were transferred electrophoretically onto EMD Millipore™ Immobilon™-P PVDF Transfer Membranes (Cat# IPVH00010, EMD Millipore™) at 20V for 1 h. Membranes were incubated for 1 hour at room temperature in blocking buffer (5% low fat powdered milk in Tris-buffered saline with 0.1% Tween20 [TBST]) and incubated overnight with antibodies at 4°C in blocking buffer. See Table 1 for sources and dilutions of all primary and secondary antibodies used for Western blotting. Membranes were washed 3 times with TBST and incubated for 30 minutes with a secondary antibody in blocking buffer at room temperature. Blots were developed using chemiluminescence (SuperSignal™ West Pico PLUS, Cat# 34577, Thermo Fisher Scientific) on FluorChem M Protein Simple detection system (San Jose, CA).

Confocal Scanning Laser Ophthalmoscopy (cSLO) and Spectral Domain Optical Coherence Tomography (SD-OCT)

Procedures for cSLO and SD-OCT have been previously described (14). In short, mice were anesthetized with ketamine (100 mg/kg) and xylazine (10 mg/kg) and eyes were anesthetized with 0.5% proparacaine hydrochloride ophthalmic solution (NDC: 17478-263-12, Akorn Inc., Lake Forest, IL). Pupils were dilated with 1% tropicamide eye drops. Ocular eye shields (33, 34) and Systane Ultra Lubricant Eye Drops (Alcon Laboratories, Inc., Fort Worth, TX) were used to keep eyes hydrated. The Spectralis HRA + OCT (Heidelberg Engineering, Inc., Franklin, MA) was used to obtain infrared reflectance (815 nm) and autofluorescence (excitation 486 nm/emission 500-680 nm) images of the retina using with a 55° wide-field objective lens. Following cSLO, imaging of retinal lamina structure was accomplished using a Bioptigen Envisu R2210 SD-OCT system (Leica Microsystems, Buffalo Grove, IL). Image J v1.52p was used to analyze cSLO images to

quantify number of hyperfluorescent foci. SD-OCT scans were quantified manually using Bioptigen Diver version 3.4.4 (Leica Microsystems, Buffalo Grove, IL). Animals were imaged at various time points within 1 week of indicated time points.

Electroretinogram

Two ERG paradigms were employed as previously described (7, 14, 26). For *RetΔGlut1* mice, after overnight dark adaptation, mice were anesthetized with sodium pentobarbital (65 mg/kg), the corneal surface was anesthetized (1% proparacaine HCl), and the pupils were dilated (1% tropicamide, 2.5% phenylephrine HCl, and 1% cyclopentolate). Mice were placed on a temperature-regulated heating pad throughout the recording session. ERGs were recorded in response to strobe flash stimuli presented in the dark by an Espion E3 ColorDome Full field Ganzfeld (Diagnosys, Lowell, MA). An Ag/AgCl electrode in contact with the cornea was referenced to an Ag/AgCl pellet electrode placed in the mouth of the mouse and a ground lead was placed in the tail of the mouse.

For *RodΔGlut1* mice, animals were first dark-adapted and then anesthetized with ketamine (80 mg/kg) and xylazine (16 mg/kg). Pupils were dilated with eyedrops as described above and mice were placed on a temperature-regulated heating pad. ERGs were recorded in response to strobe flash stimuli presented in the dark by a UTAS Bigshot ERG system (LKC Technologies, Gaithersburg, MD).

For both protocols, ten strobe stimuli ranging from −3.6 to 2.1 log candela (cd)·s/m^2 were presented in order of increasing flash strength, and the number of successive trials averaged together decreased from 20 for low-level flashes to 2 for the highest flash stimuli. The duration of the interstimulus interval increased from 4 s for low luminance flashes to 90 s for the highest stimuli. Immediately after the dark-adapted recording, a steady 20 cd/m^2 adapting field was presented in the ganzfeld bowl. After 7 minutes of light adaptation, photopic cone ERGs were recorded to strobe flash stimuli (−1 to 2 log cd·s/m^2) superimposed on the adapting field.

The amplitude of the a-wave was measured at a fixed timepoint (8.32 ms for *RetΔGlut1*; 8 ms for *RodΔGlut1*) after the flash onset from the pre-stimulus baseline. The dark-adapted b-wave amplitude was measured from the a-wave amplitude trough to the peak of the b-wave. The amplitude of the light-adapted ERG was measured from the initial negative trough to the peak of the response. For graphs presenting multiple time points, the relative scotopic a-wave, scotopic b-wave, and photopic b-wave amplitudes presented are derived from the average response to a 1.4 log cd·s/m^2 flash at each time point.

Retinal and RPE flat mounts

Enucleated eyes were immediately placed into 4% paraformaldehyde (PFA) (Cat# 15710, Electron Microscopy Sciences, Hatfield, PA) for 8 minutes. For RPE flat mounts, the mice were sacrificed 2-3 hours after lights went on in the animal facilities. The procedures for RPE flat mounts were performed as described (7, 14). For retinal flat mounts, the eyes were placed onto a dish in 1x PBS, and the cornea and lens were removed. Eyecups were placed back in 4% PFA for 8 minutes. The retinas were then carefully separated from the RPE/choroid and washed in 1x PBS. The fixed retinas were permeabilized and blocked in

5% BSA 0.1% Triton X-100 for 1 hour, then incubated in primary antibody overnight in 1% BSA + 0.1% Triton X-100 at 4°C (Table 1). The retinas were washed with PBS, and secondary antibody and DAPI was applied in 1% BSA + 0.1% Triton X-100 for 1 hour at room temperature. Retinas were then washed in PBS and placed on a glass slide. Retinas were then flattened with 4-6 radial cuts and slides were cover slipped using Gelvatol.

Image analysis and quantification

Quantification of cone arrestin positive cells was performed in Image J v1.52p (35) using the auto local threshold algorithm, followed by automated particle detection algorithms performed on thresholded images. Representative flat mount images were taken using Zeiss LSM780 NLO confocal/multiphoton microscope. Quantification of rod and cone OS lengths were performed on images from retina cryosections immunolabeled with antibodies to rhodopsin or cone opsin. Quantification was performed using ImageJ with OS position and length information stored using the ROI manager plugin. The number of TUNEL and avidin positive nuclei were manually counted within ImageJ.

RNA Isolation, cDNA Synthesis and Quantitative PCR

Neural retinas were isolated and placed immediately into 1 ml TRIzol (Cat# 15596026, Thermo Fisher Scientific), after which they were homogenized using a 1 ml syringe with a 18G needle (Cat# 305195, BD PrecisionGlide Needle), then with a 25G needle (Cat# 305124, BD PrecisionGlide Needle). RNA was extracted according to manufacturer specifications. RNA was quantified with a NanoDrop (ND-1000, Thermo Fisher Scientific). RNA (1μg) was reverse transcribed to cDNA with a final volume of 20 μl using EcoDry Premix ([oligo dT] Cat # 639543 Takara Bio U.S.A., Mountain View, CA).

cDNA derived from 1 μg of mRNA was used for qPCR and was performed with PowerUp SYBR Green Master Mix (Cat# A25742, Thermo Fisher Scientific) on a QuantStudio 5 Real-Time PCR System (Cat# A28139, Thermo Fisher Scientific). The PCR reaction was performed according to manufacturer's protocol. All primers (Table 2) were designed for an annealing temperature of 60°C. In short, reactions were heated to 50°C for 2 minutes and held to 95°C for 10 minutes. Samples were then denatured at 95°C. Cycle threshold (Ct) values were generated by the software and normalized to RPLP0. Values of $2^{-(\Delta\Delta Ct)}$ were used to compare levels of gene expression across animals.

TUNEL Assay

Cryosections from 4% PFA fixed eyes were used for the detection of apoptotic cells with ApopTag® Fluorescein *In Situ* Apoptosis Detection Kit (Millipore, Cat# S7110), following manufacturer instructions. In short, frozen sections were brought to room temperature, and a hydrophobic barrier was drawn around the entire slide using an ImmEdge Hydrophobic Barrier PAP Pen. The sections were post-fixed in an ethanol: acetic acid solution for 5 minutes at −20°C, then washed in PBS. Equilibration buffer was applied for 1 minute and aspirated. TdT enzyme was added, and sections were incubated in a HybEZ™ II Hybridization oven for 60 minutes at 37°C. Stop/Wash buffer was used, and anti-digoxigenin conjugate was applied for 30 minutes at room temperature. Slides were

then washed and counterstained with DAPI and coverslips mounted with Gelvatol. Slides were imaged using a Zeiss LSM780 NLO confocal/multiphoton microscope.

Measurement of Lactate

All steps of the assay were performed in Krebs-Ringer-Bicarbonate (KRB). KRB consisted of 98.5 mM NaCl, 4.9 mM KCl, 1.2 mM KH_2PO_4, 1.2 mM $MgSO_4$-$7H_2O$, 20 mM HEPES, 2.6 mM CaCl-$2H_2O$, and 25.9 mM $NaHCO_3$, dissolved in deionized H_2O, which was bubbled with 5% CO_2 to adjust the pH to 7.4 and filtered through a 0.22 μm membrane. Glucose was diluted with KRB solution to 5 mM (GKRB), aliquoted into 48 well plates (Cat#3548, Corning) and placed into a cell incubator at 37°C, 5% CO_2, prior to dissection. Each retina was dissected and placed in a single well of a 48 well plate in GKRB. Samples were taken after 15, 30, and 60 minutes and lactate in the GKRB was measured using Lactate Reagent (Cat#735-10, Trinity Biotech, Bray, Co Wicklow, Ireland).

Metabolomics Analysis

Animals were dark adapted for 2-3 hours and all procedures were performed in dim red light. Eyes were placed in ice cold 1x Hank's Balanced Salt Solution (Cat# 88284, Thermo Fisher Scientific) over parafilm layers. The anterior segment including lens was quickly removed and retina was separated from eyecup with fine forceps and flash frozen. Retinal metabolites were extracted and analyzed by targeted metabolomics using liquid chromatography with tandem mass spectrometry (LC MS/MS) as reported (4, 36). The peaks were integrated using multiquanta 3.0.2 software (Ab Sciex) and the peak intensities were imported into R-studio v2022.02.0 Build 443, using MetaboAnalyst package v3.2.0 (37). All metabolite levels were scaled by pareto scaling, and p-values were obtained by t-test within the package.

Statistical Analysis

All graphs and statistical analysis were done using GraphPad Prism version 9.3.0 (GraphPad, San Diego, CA). Unpaired two-tailed Student's *t*-tests were performed between samples to determine the *P* values. One-way ANOVA was performed when comparing more than two genotypes, and two-way ANOVA was performed when comparing more than two different variables. A value of $P \leq .05$ was considered significant, and represented as $P \leq .05$ *(*)*, $P \leq .01$*(**)*, $P \leq .001$ *(***)*, $P \leq .0001$*(****)*. All ERG data are graphed as mean ± SEM $N \geq 3$, and all other data was graphed as mean ± SD $N \geq 3$.

Data Availability

The data that support the findings of this study are available on request from the corresponding author.

Results

GLUT1 and GLUT3 are the primary glucose transporters in the Neural Retina

Glucose is the primary metabolic substrate of the neural retina and is transported across the inner and outer blood-retinal barrier by GLUT1. The RPE forms the outer blood-retinal

barrier and transports ~60-70% of the glucose entering the retina, where it can be utilized for anabolic and catabolic metabolism (1, 7). To better understand the expression levels and cell specificity of the different glucose transporters in the retina, we analyzed scRNAseq libraries from 1 month old mouse neural retina (GSE153673; 28) for genes that encode proteins with glucose transmembrane transport activities (GO:5355). We found that *Slc2a1* (encoding GLUT1) and *Slc2a3* (encoding GLUT3) had the highest expression in the retina (Figure 1A). While *Slc2a1* was expressed in all retinal cells analyzed, its expression was the highest in Müller glial cells (MGCs). Furthermore, *Slc2a1* was the only transporter with high expression in rods, cones and MGCs. In contrast, *Slc2a3* is expressed robustly in horizontal cells, amacrine cells, bipolar cells, and ganglion cells, but expression is low in MGCs or photoreceptors. To validate the RNAseq analysis for *Slc2a1* and *Slc2a3*, we performed *in situ* hybridization on frozen sections of 1-month-old control retinas. The *Slc2a1* RNAscope probe labeled the RPE, inner segment layer (IS), outer nuclear layer (ONL), inner nuclear layer (INL), and the ganglion cell layer (GCL). In contrast, the *Slc2a3* RNAscope probe was primarily detected in the INL, and GCL (Figure 1B) consistent with previous reports (38, 39). Multiple cell types reside in the GCL apart from ganglion cells (including displaced amacrine cells, astrocytes and MGC end feet) all of which could express *Slc2a3*. Taken together our data show that GLUT1 is the major glucose transporter of the outer retina.

Expression of *Slc2a3* does not compensate for loss of *Slc2a1* in the outer retina of *RetΔGlut1* mice

To investigate whether GLUT1 expression in the neural retina supports visual function, we characterized transgenic mice with a pan retinal knockout of *Slc2a1* (*RetΔGlut1*), generated by crossing the $Glut1^{flox/flox}$ mouse to *Crx-Cre* transgenic mice (26, 40). To confirm excision of the *Slc2a1* gene in *RetΔGlut1* mice, we examined the expression of *Slc2a1* by *in situ* hybridization in retinas from 1-month-old mice. In control mice, *Slc2a1* was detected in the inner retinal blood vessels, IS, ONL, INL and GCL (Figure 2A, left panel) as previously shown (Figure 1B). In the *RetΔGlut1* retina the signal was lost from the IS, ONL, INL and GCL, but *Slc2a1* was still detected in inner retina blood vessels (arrows in Figure 2A, right panel). Sporadic *Slc2a1* signal was seen in the ONL, most likely due to mosaic expression of *Cre* (40).

Localization of GLUT1 protein was examined by immunolabeling retinal cryosections from control and *RetΔGlut1* mice (Figure 2B). In control mice the brightest labeling was observed in the basolateral and apical membranes of the RPE, retinal capillaries, and MGC somas and their processes in the INL and ONL (Figure 2B) as described previously (7, 26, 41, 42). Faint GLUT1 labeling was also detected in the IS, consistent with its distribution in photoreceptors (7, 26, 41). In comparison, GLUT1 immunolabeling was mostly absent from the retinal layers of *RetΔGlut1* mice but was detected in the RPE and inner blood vessels. Consistent with the *in-situ* data, GLUT1 staining was detected only sporadically in MGCs or photoreceptors in the outer retina.

To determine whether *Slc2a3* was increased to compensate for the loss of *Slc2a1* we performed *in situ* analysis with probes for *Slc2a3*. In the *RetΔGlut1* the expression pattern was similar to that of control with most of the signal restricted to the INL and GCL

along with a small scattering of signal in the ONL (Figure 2C). Immunolabeling of retina cryosections was performed to confirm that expression of GLUT3 was not altered in *RetΔGlut1* mice. In the control retinas, the highest GLUT3 expression was restricted to two bands within the IPL (Figure 2D). Previous studies have shown GLUT3 to colocalize mainly to two bands within the IPL that were identified as amacrine cells based on their immunolabeling for choline acetyltransferase (38, 39). In *RetΔGlut1* mice the pattern of staining for GLUT3 did not change (Figure 2D right panel). Loss of GLUT1 expression from P20 *RetΔGlut1* retinas was confirmed by immunoblot analysis of whole retina (Figure 2E). Additionally immunoblot analysis confirmed that GLUT3 expression levels are not altered in retinas of *RetΔGlut1* mice (Figure 2F). Taken together these results show that GLUT1 is the primary facilitative glucose transporter in the outer retina, while GLUT3 expression is restricted to the inner retina. Our results confirm the ablation of GLUT1 expression in the *RetΔGlut1* retina and indicate that GLUT3 does not compensate for loss of GLUT1 in the outer retina.

Photoreceptor degeneration in *RetΔGlut1* mice

As *Crx Cre* is expressed throughout the neural retina (40), the loss of glucose uptake may have a global impact on the neural retina. We used SD-OCT to monitor longitudinal changes in the retina between P20 and 4 months of age. Representative B-scans from the horizontal meridian are shown for 2-month-old control and 1-, 2-, and 4-month-old *RetΔGlut1* eyes (Figure 3A). Progressive thinning of the ONL was apparent in *RetΔGlut1* mice from 1 to 4 months. The *RetΔGlut1* photoreceptor lamina were also observed to have lower bright/dark signal contrast than controls indicating less signal/back-reflection from locations corresponding to the outer limiting membrane (OLM), IS/OS transition zone and photoreceptor OS apical tips (Figure 3A). To track the progression of ONL layer changes, the ONL thickness was quantified from control and *RetΔGlut1* mice from P20 to 4 months of age (Figure 3B). The *RetΔGlut1* ONL was reduced by ~18% of control at 1 month and by 45% of control by 4 months of age (Figure 3B). In contrast, the inner retinal layer thickness measured from the OPL to the innermost GCL reflectance signal was not different in *RetΔGlut1* at any age (Figure 3C).

RetΔGlut1 mice have impaired visual function

The impact of GLUT1 deletion on retinal function was investigated using ERG analysis. Dark-adapted (rod photoreceptor driven) a-wave amplitudes were reduced in 1 month old *RetΔGlut1* mice (Figure 3D). We next compared amplitudes for responses to stimuli that elicited a near-maximal response in controls and *RetΔGlut1* at different ages. At P20, near the time of first eye opening, the response amplitude was not altered in *RetΔGlut1* mice. At 1 month of age, however, a-waves were ~25% of control (132 μV ± 16 vs 508 μV ± 30, mean ± SD) (26). Between 2 and 4 months, a-wave amplitudes were reduced further to less than 20% of control (Figure 3E). Dark-adapted b-waves were reduced in a similar manner, likely due to the much-diminished photoreceptor activation of bipolar neurons.

We next examined the thickness of the OS layer in B-scans as photoreceptor OS maintenance has been shown to depend on glycolytic pathways (8, 12, 21). In control mice the OS layer thickness increased from P20 to 1 month and was then maintained at ~25 μm

throughout adulthood. In contrast, *RetΔGlut1* OS thickness was ~15% less than controls at P20, and failed to further increase in length during late post-natal development (Figure 3F). Our data suggest that glucose uptake via GLUT1 is necessary for the normal elaboration and maintenance of the photoreceptor OS.

Previous studies have shown that cones are less dependent on glycolysis than rods in non-degenerating retinas (6, 14, 43). However, in models of RP, cones maintain their viability by upregulating aerobic glycolysis through stabilization of GLUT1 expression at the plasma membrane of cone photoreceptors (2, 6). Given that cones represent only 3% of photoreceptors in the mouse retina, it is difficult to assess impacts to cone viability with SD-OCT. To examine if loss of cone photoreceptors contributed to the observed thinning of the *RetΔGlut1* ONL, 4-month-old retinal flat mounts were immunolabeled for cone arrestin (ARR3) to quantify cone density (Figure 4A). Surprisingly, there was no difference in cone density in retinas from 4-month-old control and *RetΔGlut1* mice (Figure 4A right panel). To investigate the impact of GLUT1 loss on cone function, cone-driven responses were isolated by superimposing stimulus flashes on a rod-desensitizing background (Figure 4B). Photopic (cone-driven) b waves were reduced in *RetΔGlut1* mice at 1 month but less so compared to the dark-adapted responses. Maximum cone-driven response amplitudes were not different at P20 but were reduced to 62% of control at 1 month of age and to 46% of control at 4 months (Figure 4C). The data suggest that cones of *RetΔGlut1* mice do not die although cone visual function is impaired with loss of GLUT1.

RetΔGlut1 mice have arrested OS development

The ERG deficits observed in *RetΔGlut1* mice were more severe than predicted by photoreceptor loss alone (Figure 3B and D). For example, at 1 month of age, ONL thickness was reduced by 18% while the maximal a-wave responses were reduced by ~75%. Furthermore, while the number of cones did not change (Figure 4A), photopic b-wave responses were reduced by ~40% (Figure 4B, C). Measurements from SD-OCT suggested that OS lengths were shorter (Figure 3F). Since OS measurements from OCT are sensitive to fluid levels and cone OSs cannot be measured by OCT, immunolabeled cryosections were used to quantify the lengths of rod and cone OSs and examine the localization of opsin.

We quantified the OS length of rods and cones by staining, respectively, for rhodopsin (RHO) and mid-wave cone opsin (M-opsin) at P12, when the highly organized disc architecture of the OS begins to take shape (44-46) and at P30, when OSs have assumed their adult length and structure, (Figure 5A, B). RHO was localized to the OS in both control and *RetΔGlut1* mouse at both ages (Figure 5A). At P12, rod OS lengths were not significantly different between control and *RetΔGlut1* mice, indicating that initial OS formation is not impacted by lack of GLUT1 (Figure 5A). By P30, however, *RetΔGlut1* rod OSs were ~50% shorter than those of controls (Figure 5A), in agreement with our SD-OCT results (Figure 3F) and suggesting that rod OS formation is slowed in the absence of GLUT1. Similarly, M-opsin was localized to the OS in both control and *RetΔGlut1* mice at both P12 and P30 (Figure 5B) and cone OS length was not significantly different at P12, although fewer M-opsin positive cones were seen at P12, despite controlling for orientation of cryosections. At P30, although we no longer observed a decreased density of cones in the

RetΔGlut1 retina, the length of their OS was only ~50% of control. These data indicate that the rate of nascent cone OS formation may be slowed in the absence of GLUT1 such that they never achieve a fully formed OS at any age.

Opsin protein biosynthesis is a driver of OS formation, and disc morphogenesis is disrupted in photoreceptors with low opsin levels (47-49). Intermediates of glucose metabolism serve as precursors for synthesis of nucleotides, amino acids and glycans, and anabolic impairments in OS renewal were observed in models with disrupted glycolytic enzymes (8, 9, 12, 21, 50). Therefore, we tested whether shortened OSs resulted from impaired protein biosynthesis in *RetΔGlut1* mice. Total levels of RHO were examined at P12, P20 and P30 (Figure 5C). These ages were chosen to correspond to eye opening (P12), partial elaboration of the OS (P20) and the presence of a mature OS with adult RHO concentration (P30) in wild type mice (51, 52). Retinal lysates from control and *RetΔGlut1* were run on polyacrylamide gels and blotted for GLUT1, RHO and Rod arrestin (ARR1) (Figure 5C). While RHO levels were clearly reduced, ARR1 levels were similar between controls and *RetΔGlut1* at all ages examined (averaging 92-96% of controls). Since there was no difference in ARR1 levels between controls and *RetΔGlut1* mice, we examined how the absence of retinal GLUT1 impacted the ratio of RHO to rod arrestin (RHO/ARR1) (Figure 5C). At P12 there was no difference in the RHO/ARR1 ratio between control and *RetΔGlut1* mice. However, by P20, RHO/ARR was decreased in the *RetΔGlut1* retina to ~50% of control (0.85 ± 0.08 vs 1.67 ± 0.29) and further decreased to 33% of control (0.58 ± 0.2 vs 1.78 ± 0.35) at P30 (Figure 5C). These data indicate that in the absence of GLUT1 and low glucose availability, synthesis of membrane glycoproteins (RHO) is reduced more than synthesis of cytoplasmic proteins.

We next tested the possibility that lower levels of RHO at 1 month of age was the result of reduced transcription. Our qPCR data showed that transcription of *Rho* but not *Arr1* was reduced by ~50% in *RetΔGlut1* (Figure 5D). Thus, reduced RHO results in part from reduced transcription of *Rho*. However, we observed normal levels of ARR1 protein and *Arr1* transcript.

We next examined whether cones have similar anabolic impairments as rods of *RetΔGlut1 mice* by measuring relative expression of M-opsin at P30 (Figure 5E). M-opsin levels of 1-month-old *RetΔGlut1* mice were 50% of controls (Figure 5E) while there was no difference in the expression of M-Opsin mRNA, encoded by the *Opn1mw gene,* between control and *RetΔGlut1* mice (Figure 5F). Moreover, expression levels of cone arrestin, (ARR3), encoded by *Arr3*, were not significantly decreased in the *RetΔGlut1* retina. Our data show that in the absence of GLUT1, transcription of *Rho* but not *Opn1mw* is impaired, and that the expression of both proteins is dependent on glucose uptake.

If biosynthetic pathways for OS constituents were slowed during synthesis or maturation, due to limited availability of anabolic building blocks, we might expect increased localization of opsins in non-OS compartments. We examined the localization of rhodopsin and cone opsins by adjusting the display gain equivalently across images to amplify signal from non-OS photoreceptor regions. We noted increased immunolabeling for rhodopsin and cone opsin in photoreceptors of *RetΔGlut1* but not control mice (Supplementary Figure 1A,

B), suggesting that sluggish biosynthesis of glycoproteins in the absence of GLUT1 results in aberrant localization of opsin to non-OS compartments.

The shortened OS length suggests that OS renewal is impaired in *RetΔGlut1* photoreceptors due to anabolic deficits. However, there is a possibility that engulfment and phagocytosis of OS tips by the RPE is also disrupted in *RetΔGlut1* mice. We investigated the possibility of altered uptake of OS discs in *RetΔGlut1* mice by immunolabeling RPE flat mounts for RHO and ZO1, an RPE tight junction - specific marker. The RPE was isolated at 2.5 hours after lights on, corresponding to the diurnal peak in number of internalized phagocytosed OS in the RPE (53). We find numerous rhodopsin positive inclusions in the RPE from P20 and P30 *RetΔGlut1* with comparable densities to that of control RPE (Supplementary Figure 2), suggesting that phagocytosis of OS by the RPE is normal.

Inflammation accompanies photoreceptor degeneration in *RetΔGlut1* mice

Photoreceptor degeneration is frequently accompanied by microglia activation and immune cell infiltration into the subretinal space (54, 55). To examine the involvement of inflammation and its temporal relationships to cell degeneration and loss, we used cSLO with blue light stimulation to capture autofluorescence (BAF) in *en face* scans of *RetΔGlut1* and control retinas (Figure 6A). BAF scans revealed hyperfluorescent foci (HF) in the *RetΔGlut1* retina at 1 month of age which became more numerous in older animals (Figure 6A, B). HF have been correlated to infiltrating microglia and/or macrophages in the outer retina (56, 57). To verify that HF foci corresponded to microglia and/or myeloid cells, retina cryosections were labeled with an antibody to Iba-1 (Figure 6C). We found Iba-1 labeled cells in the outer retina of *RetΔGlut1* but not of control mice. At 1 month of age these were more likely to be localized to the OPL; by 4 months we noted their infiltration into the sub-retinal space.

To better understand the timing and location of the degenerative changes indicated by SD-OCT, we performed TUNEL assays on retinal sections from *RetΔGlut1* and control mouse eyes at P15 and P30 (Figure 6D). *RetΔGlut1* photoreceptors undergo cell death as early as P15, as numerous TUNEL positive cells were detected in the ONL but not in the INL or GCL (Figure 6D). We observe similar patterns and number of TUNEL positive cells in the ONL of P30 *RetΔGlut1* retina (data not shown). The ONL specific TUNEL signal suggests that photoreceptors require GLUT1 for survival, and that cell death occurs during post-natal and adult stages.

Since the glycolytic intermediate glucose-6-phosphate (G6P) is used in the pentose phosphate pathway for the renewal of NADPH, a key electron donor in the cell's antioxidant defense system, loss of GLUT1 in the outer retina would inhibit this system leading to oxidative stress resulting in cell death. To test the hypothesis that elevated oxidative stress contributes to the photoreceptor degeneration observed in *RetΔGlut1* mice, cryosections were stained with avidin, a probe for oxidative DNA damage (58, 59). At P15 when elevated TUNEL staining was observed, there were numerous avidin-positive cells in the *RetΔGlut1* ONL that were only rarely encountered in control retinas (white arrows indicate representative avidin positive nuclei, Figure 6E), indicating that reduced glucose uptake elevates oxidative stress leading to photoreceptor degeneration. No differences in avidin

staining of INL and GCL were observed between control and *RetΔGlut1* mice, consistent with the lack of TUNEL-positive cells in these retinal cell layers.

Retinas lacking GLUT1 have an altered metabolic profile

Studies with isolated retinas demonstrate that large amounts of lactate are released when glucose is present in the media (60-62). The high rate of aerobic glycolysis has been attributed to photoreceptors despite the fact that *Slc2a1* expression is higher in MGCs (Fig. 1A). To investigate the impact of *Slc2a1* deletion on the rate of aerobic glycolysis, lactate efflux was measured from the media after incubation of neural retinas for 1 hour with Ringer's buffer supplemented with 5 mM of glucose. Isolated *RetΔGlut1* retinas released 4-fold less lactate in comparison to controls (Figure 7A) indicating that retinal aerobic glycolysis depends on glucose uptake via GLUT1.

To understand how restricted glucose uptake affected metabolic pathways in the retina, targeted steady state metabolomics was undertaken with LC MS/MS focusing on amino acids, tricarboxylic acid cycle (TCA) metabolites, nucleotides, and carnitines from 1-month-old control and *RetΔGlut1* neural retinas. A multivariate analysis, Partial Least-Squares Discriminant Analysis (PLS-DA), was used to determine if *RetΔGlut1* neural retinas were different from the controls. Control and *RetΔGlut1* retinas form two distinct clusters indicating an overall difference in their metabolic profiles (Figure 7B). Next, to understand the significant differences between controls and *RetΔGlut1* neural retinas, we performed t-tests from normalized LC MS/MS values and identified 17 significantly changed metabolites out of 90 measured metabolites (Figure 7C). A heatmap of the top 25 metabolites was generated based either on the statistical significance or degree of fold change (Figure 7D).

Lactate levels were lower in *RetΔGlut1* samples, consistent with our efflux measurements and with reduced retinal glycolysis. The TCA cycle intermediate succinate was decreased, while aspartic acid, a derivative from the TCA cycle, had increased abundance. Mitochondrial acyl-carnitines (AC) serve as the precursors for fatty acid oxidation (FAO) that could meet the energetic needs of the neural retina. We found a decreased abundance of propionyl-, isobutyryl-, butyryl-, and stearoyl-carnitine species (Figure 7C, D) in the *RetΔGlut1* mouse suggesting enhanced FAO. Proline levels were significantly decreased (Figure 7C) suggesting an increase in proline catabolism. The metabolic profile of the *RetΔGlut1 retina* is characterized by depletions in AC which are suggestive of increased amino acid catabolism and FAO in the absence of GLUT1 transport activity.

Rods depend on glucose uptake through GLUT1 for normal visual function and viability

The impairment of visual function in *RetΔGlut1* mice could result from lack of glucose uptake into photoreceptor cells directly. Conversely, it could also result secondarily from lack of glucose transport into MGCs, as they can generate metabolites from glucose to support photoreceptor function (10, 50, 63, 64). To distinguish these possibilities, we investigated the functional and structural impact of *Slc2a1* deletion in rods by crossing $Glut1^{flox/flox}$ mice with transgenic mice having tamoxifen inducible *Cre* expressed under the control of the rod *Pde6g* promoter (*RodΔGlut1*). To confirm the deletion of GLUT1 from rods, we performed *in situ* hybridization and immunohistochemistry in control and

RodΔGlut1 retinas 1 month after tamoxifen induction (Figure 8A, B). We noted a loss of signal from the *Slc2a1* RNAscope probe from the ONL and IS layer in *RodΔGlut1* retinas (Figure 8A). Similarly, reduction in signal by anti-GLUT1 immunolabeling was seen in the IS, ONL and OPL. The remaining GLUT1 staining can be attributed to the MGC apical processes (Figure 8B).

It has been known that GLUT1 protein is highly expressed in the neural retina, however it was not known how much of the signal was attributed to photoreceptors. To quantify the relative contribution of rods to total retinal GLUT1 levels, western blot analysis for GLUT1 from 1 month old control, *RetΔGlut1* and *RodΔGlut1* retinas was performed, with vinculin serving as control (Figure 8C). The western blot quantification showed that GLUT1 expression is reduced by ~20% in *RodΔGlut1* mice. The larger GLUT1 reduction seen in the *RetΔGlut1* model, by ~85% of control, indicates that rod photoreceptors account for a modest fraction of total GLUT1 present in the neural retina.

To gain insight into whether glucose directly or indirectly supports rod photoreceptor cells, we measured the structural and functional changes in retinas of 1-month post tamoxifen-treated control and *RodΔGlut1* mice. ONL thickness and rod OS length were measured from cryosections that were immunolabeled with RHO and DAPI (Figure 8D). ONL thickness of *RodΔGlut1* was not altered, however OS length was ~70% of that of controls. ERG a-waves were reduced in *RodΔGlut1* retinas as were ERG b-waves (Figure 8E). In comparison, photopic b-waves reflecting function of the cone pathway revealed modest changes in amplitude (Figure 8F). We compared peak a-wave and peak scotopic and photopic b-wave amplitudes elicited by 1.4 cd s /m^2 flash stimuli (Figure 8G). The kinetics of the leading edge of the a-wave were comparable to control in both the *RetΔGlut1* and *RodΔGlut1* mice, indicating that rods retained normal phototransduction in the absence of GLUT1 (not shown). Scotopic a-waves were reduced by 40% (233 μV ± 94 vs 383 μV ± 82, mean ± SD), b-waves were reduced by ~30% (794 μV ± 189 vs 1180 μV ± 241, mean ± SD) and photopic b-waves were reduced by ~25% (231 μV ± 19 vs 304 μV ± 58, mean ± SD). Our data indicates that glucose uptake into rods is required for rod function, and that cones depend on a metabolite derived from glycolysis in rods. Finally, western blot analysis for RHO, and ARR1 revealed that RHO protein levels were reduced to 50% of controls while ARR1 was not changed significantly (Figure 8H).

In both *RetΔGlut1* and *RodΔGlut1* mice, there were changes in OS length and RHO protein expression. However, in contrast to *RetΔGlut1* mice, the ONL thickness of *RodΔGlut1* remained unaltered at 1 month of age while the ONL of *RetΔGlut1* mice was reduced by 20%. The comparisons of functional and structural parameters in *RodΔGlut1* and *RetΔGlut1* mice indicate that rod photoreceptors require the direct uptake of glucose via GLUT1. Responses of photoreceptors to glucose deprivation were similar in *RodΔGlut1* and *RetΔGlut1* mice, although the magnitude of impairments were greater for *RetΔGlut1* at 1 month. However, the *RodΔGlut1* model was generated by tamoxifen induced Cre activation at 1 month of age. Since the *Cre* expressed in our *RetΔGlut1* line is not dependent on tamoxifen for activity and is turned on early in development, the timing of Cre - mediated excision and full GLUT1 ablation may differ in the two models. Therefore, we examined the impacts to retinal structure and anatomy with SD-OCT at 4 months

post-tamoxifen injection in our *RodΔGlut1* mice and compared this with 4-month-old *RetΔGlut1* mice. (Supplemental Figure 3A). As shown for *RetΔGlut1* mice (Figure 3A) we observe attenuated reflectivity in B-scans of *RodΔGlut1* mice corresponding to the OLM, the photoreceptor transition zone and OS tips. ONL thinning is comparable in both *RetΔGlut1* and *Rod ΔGlut1*. cSLO images show numerous BAF foci in *RodΔGlut1* 4 months post-tamoxifen, akin to that of the 4-month-old *RetΔGlut1* (Supplementary Figure 3B). We quantified the ONL thickness from SD-OCT scans of *RodΔGlut1* and compared this to *RetΔGlut1* and controls (Supplementary Figure 3C). ONL thickness was reduced by 41% in *RodΔGlut1* at this timepoint, similar to the 45% reduction in *RetΔGlut1* mice. We also quantified the OS layer thickness from B-scans of *RodΔGlut1* mice and observed a 60% decrease in both *RodΔGlut1* and *RetΔGlut1* mice (Supplementary Figure 3D). We also quantified the number of BAF spots in cSLO images from *RodΔGlut1* and found a similar number of foci compared with *RetΔGlut1* (Supplementary Figure 3E). Taken together our data argue that glucose uptake in rods is required for OS biosynthesis and viability in a cell autonomous manner.

To confirm that BAF foci observed in *RodΔGlut1* originate from microglia as was the case for *RetΔGlut1* mice, cryosections of 4-month post-tamoxifen *RodΔGlut1* and 4-month-old *RetΔGlut1* mice were immunolabeled with Iba-1 (Supplementary Figure 4A). We observed Iba-1 positive cells throughout the photoreceptor layer of both *RetΔGlut1* and *RodΔGlut1* mice, indicating increased microglia infiltration accompanying photoreceptor degeneration in these models. Reactive gliosis is often observed in retinas undergoing photoreceptor degeneration and is readily observed using GFAP immunolabeling. We find elevated GFAP in both *RodΔGlut1* and *RetΔGlut1* retinas (Supplementary Figure 4B).

Discussion

Glucose is an essential metabolite for the neural retina, where it is used to fuel high rates of glycolysis and mitochondrial respiration (4, 62). Reduced transport of glucose into the outer retina is implicated in photoreceptor loss in animal models of human RP (3). Therefore, an understanding of the glucose transporters expressed in the neural retina and the impact of glucose deprivation is needed to develop rational treatment strategies to repair nutrient imbalances and prevent photoreceptor cell death. In this study we determined that *Slc2a1*, encoding for GLUT1, was the primary glucose transporter in the outer retina and used conditional targeting to ablate *Slc2a1* from all retinal neurons and glia (*RetΔGlut1*) or only from rod photoreceptors (*RodΔGlut1*). Pan-retinal deletion of GLUT1 resulted in impairments in opsin biosynthesis and OS renewal in photoreceptors which contributed to rod photoreceptor death. Rod-specific deletion resulted in similar impairments in OS renewal, but rod cell death was not initially observed.

GLUT1 is an essential transporter in the outer retina

The *RetΔGlut1* retina appeared normal at P12 but displayed progressive thinning of the ONL at later ages and elevated apoptosis was observed as early as P15. No thinning or TUNEL staining was detected in the INL or GCL at any age. *Slc2a3* encodes GLUT3, a high affinity and high-capacity glucose transporter, which is expressed in tissues having lower interstitial

glucose concentration compared with blood, such as the brain (65). GLUT3 is present in the inner retina (38, 39) and *in situ* Western blotting and immunofluorescence data showed that photoreceptors do not upregulate *Slc2a3* expression to compensate for deletion of *Slc2a1* (Figure 2D, E). The lack of inner retinal cell loss indicates that glucose uptake via GLUT3 supports the viability of inner retinal cells.

Photoreceptors differentiate normally in *RetΔGlut1* mice

In *RetΔGlut1* mice, *Cre* expression is driven by the *Crx* promoter that turns on beginning at E12.5 in photoreceptor progenitors of the outer neuroblast layer (66, 67). However, *Crx* expression is sparse at E12.5 and corresponds to a small population of early born photoreceptors. *Crx* expression does not peak until P6, when most rods have been born (66-68). Consistent with this spatiotemporal timing of Crx activity, we observe significant residual expression of GLUT1 at P3. By P10 GLUT1 expression declined and was only encountered in isolated patches within the retina (data not shown). A delay in the complete turnover of residual GLUT1 after *Slc2a1* gene excision may explain prolonged GLUT1 expression in the early post-natal *RetΔGlut1*.

It is interesting that all *RetΔGlut1* photoreceptors appear to differentiate normally and begin to form an OS. However, overall energy expenditures may be relatively low before eye opening as rod photoreceptor OS formation is not initiated until ~P10 (46, 52). The largest share of ATP consumption in the retina is from ATPase pumps that maintain the ion gradients to enable neuronal signaling (69). The light responses recorded from photoreceptors of 2-week-old mice are very small, and a fully mature OS structure is not achieved until mice are 3 weeks old (51, 70, 71). Thus, lower ATP consumption during neonatal development may allow diversion of metabolites toward the anabolic requirements of building an OS. In addition, nursing neonates may rely more on alternative fuel sources such as ketones from the mother's milk (72).

Rods and cones depend on GLUT1 activity for outer segment renewal

Though photoreceptors are non-dividing cells, the daily renewal of their OSs imposes a high biosynthetic demand. In this study we showed that in the *RetΔGlut1* mice, photoreceptor OSs never reach adult length and *RodΔGlut1* mice have shortened OSs (Figure 5A, B). At P12, rod and cone OS lengths in *RetΔGlut1* mice were not significantly different from controls. By P20, however, OS length lagged in *RetΔGlut1* mice (Figure 3F) and RHO levels were already 50% lower than in controls (Figure 5C).

RHO constitutes ~90% of OS protein and achieving a full-length OS depends on sustaining a high level of RHO synthesis (47, 48, 73). In *RetΔGlut1* mice the OS did not increase in length after P20 while control OSs continued to grow to their full adult length (Figure 3F). Based on our observations of normal numbers of RHO positive foci within the *RetΔGlut1* RPE after peak phagocytosis (Supplementary Figure 2), we can assume that the rate of OS shedding has not been altered. Our data suggests that a decreased rate of opsin synthesis impairs OS renewal by lowering the rate of basal OS replacement. Rod photoreceptors can make a light responsive OS with less than 15% of the normal opsin expression, however this low-level opsin expression results in rod death (73-75). Therefore, the rod

cell death observed in the *RetΔGlut1* mouse could be secondary to decreased rhodopsin. By 1 month, ERG amplitudes were greatly reduced in *RetΔGlut1* mice (Figure 3D, E). This reduction reflected ONL thinning (by ~20%) and shortened OSs (by ~50%) and reduced RHO expression.

OS renewal depends on anabolic building blocks (e.g., amino acids, lipid precursors) derived from glucose metabolism. Both the *RetΔGlut1* and *RodΔGlut1* mice phenocopy the defects observed when GLUT1 was knocked out of *RPE,* which resulted in shortened OS and photoreceptor degeneration (7). Taken together these findings support the model in which glucose is taken up by the RPE from the choroidal blood supply by GLUT1 at the basal membrane, delivered to the subretinal space by apical RPE GLUT1 and then is transported into rod photoreceptors via GLUT1. Our study demonstrates that glucose is an obligatory carbon source for rod photoreceptor cell OS maintenance and viability.

Impairments in OS formation have been observed in mice with rod specific ablation of genes encoding glycolytic enzymes such as lactate dehydrogenase A (LDHA), hexokinase 2 (HK2), or pyruvate kinase muscle isozyme 2 (PKM2) (9, 11, 12, 21). When we ablated *Slc2a1* specifically in rods, OS length was reduced by 34% of control and a-wave amplitudes were comparably reduced. The impaired OS renewal observed in *RodΔGlut1* mice most closely resembled the 20-50% reduction in OS length observed in the rod – specific HK2 conditional knockout (12), as opposed to the milder phenotype seen in conditional knockout of PKM2 in rods (9). This may not be surprising considering HK is the very first enzyme in glycolysis and that in *RodΔGlut1* photoreceptors we are restricting access in rods to the substrate itself. However even in HK2 knockout rods, the impact was only seen in aged mice (11, 12). In contrast, photoreceptor OS length was reduced soon after short hairpin RNA was used to ablate PKM2 or LDHA expression (21). This suggests that with conditional gene targeting strategies, developmental compensatory upregulation of isozymes (e.g., HK1) can partially overcome deficits caused by the gene deletion, whereas this may not occur with overexpression of short hairpin RNAs that interfere post-transcriptionally.

Possible influence of glucose availability on rhodopsin transcription

We found reduced transcription of rhodopsin but not cone opsin, suggesting that biosynthesis of rod but not cone OS results in part from impaired opsin transcription. A reduction in transcript levels of rod-specific proteins might be expected in 1 month old *RetΔGlut1* mice, given the observed loss of ONL thickness at this age. However, it is possible that rhodopsin transcription is repressed in response to the altered metabolic state in *RetΔGlut1* mice. For example, Krüppel - like factor 15 (KLF15) represses transcription of both rhodopsin and IRBP by binding to their promoters (76, 77). While KLF15 is normally not expressed in differentiated photoreceptors, it is induced in muscle by prolonged fasting and exercise, where it acts as a transactivator of GLUT4 expression and regulates the expression of mitochondrial Acetyl-CoA synthetase 2 (78-80). Thus, we can speculate that expression of KLF15, or that of another transcriptional silencer of rhodopsin responsive to nutritional state, could be induced in glucose - depleted rods.

Rods but not cones require GLUT1 for survival

RetΔGlut1 mice showed a selective loss of rod photoreceptors despite GLUT1 ablation from both rods and cones. The demise of rods in *RetΔGlut1* mice is accompanied by increased ONL staining for avidin, a marker of oxidatively damaged DNA, suggesting that glucose is required for protection from oxidative stress in rods. In contrast, cone viability was unaffected in *RetΔGlut1* mice at 4 months of age when marked rod degeneration was observed.

While cone function was compromised due to shortened OS (Figure 5B), the degree of cone survival was surprising, since it has been reported that cones require the upregulation of aerobic glycolysis to prolong their survival (2, 3, 81). In mouse models where a genetic mutation causes rod photoreceptor cell death, rods upregulate the secretion of a thioredoxin – like protein (rod derived cone viability factor, RdCVF) that is thought to bind to cones via Basigin 1, in order to stabilize GLUT1 in the plasma membrane of cones (2). This mechanism allows continued cone survival in the face of rod degeneration. At late-stage RP, cones lose this trophic support and die. AAV mediated overexpression of RdCVF is able to rescue cone photoreceptors in late-stage RP (2). While neither the *RetΔGlut1* nor the *RodΔGlut1* mouse is a model of RP, we observed that during rod degeneration, GLUT1 was not needed to maintain cone survival, suggesting there may be an alternative mechanism of RdCVF mediated cone survival.

In a non-diseased rod dominant retina it was proposed that cones may rely more on oxidative phosphorylation than on glycolysis (6, 43). A recent study using the *rd10* mouse showed exogenous lactate was sufficient to promote cone survival when TCA cycle activity was boosted by overexpression of a thioredoxin interacting protein (*Txnip)* allele. The rescue was also dependent on LDHB, which catalyzes the conversion of lactate to pyruvate (82). Cones of *RetΔGlut1* mice have impaired glucose uptake and also face lower overall retinal lactate. There are several possible sources for metabolites supporting cone survival in this unique context. One possibility is that cones receive sufficient lactate (or pyruvate) from microglia, as activated microglia have been shown to upregulate aerobic glycolysis (83). During retinal degeneration, microglia localized to the ONL and subretinal space may provide cones with lactate and be benefical to their initial surival. The nature of the metabolic supports for cones in *RetΔGlut1* awaits further study.

Targeted metabolomics indicate a shift in substrate utilization in *RetΔGlut1* mice

The *RetΔGlut1* neural retina metabolome showed reduction in various acyl carnitines (Figure 7), a phenomenon also reported in mice with a retinal or rod specific knockout of *Mpc1* or *Vldlr* (5, 84). Our metabolomic analysis reflects steady state levels of retina derived metabolites, so decreases could arise from reduced synthesis or increased utilization. Decreased nicotinamide riboside and pantothenic acid is consistent with an increased reliance on FAO in the retina in the absence of GLUT1 expression. Nicotinamide riboside is a salvageable NAD+ precursor providing a source of additional NAD^+ required for FAO (85, 86). Pantothenic acid is a precursor in the synthesis of CoA, necessary for activation of acyl groups for FAO. Reduced propionyl- and isobutyryl- carnitines are suggestive of not only enhanced FAO, but also increased branched chain amino acid catabolism (87, 88). Reduced

abundance of acylcarnitines, nicotinamide riboside, and pantothenic acid suggest elevated FAO in the *RetΔGlut1*. Alternatively, the lower abundance of acetyl groups (in carnitines and as acetyl-CoA), may highlight lower overall rates of lipid synthesis in the limited glucose supply of *RetΔGlut1* mouse outer retina. Lower phospholipid availability could explain the selective impairment in synthesis of membrane glycoproteins (photoreceptor opsin) compared with soluble proteins of similar cellular abundance in *RetΔGlut1* mice (ARR1) (Figure 5C).

We also observe elevated aspartate levels in retinas of *RetΔGlut1* mice, which could result from depleted pyruvate levels and therefore less acetyl-CoA available to enter the TCA. The resultant accumulation of oxaloacetic acid would be expected to result in excess transamination to aspartate, as is the case in the retina – specific MPC1 knockout (4). Accumulation of aspartate suggests that alternative fuels in the *RetΔGlut1* retina are insufficient to support metabolic needs.

The decreased abundance of proline in the *RetΔGlut1* retina suggests that proline use may be elevated to replenish depleted metabolites, such as pyruvate, in the absence of GLUT1. Proline is a key nutrient for the RPE, where it is catabolized in mitochondria to produce glutamate, α-ketoglutarate and pyruvate, which are secreted to fuel the retina (36). Proline is taken up by the retina but at a much slower rate compared with RPE (36). Activity of the first enzyme in proline catabolism, proline dehydrogenase, is lower in retina compared with RPE due to repression by high lactate and succinate (89, 90). However, in the *RetΔGlut1* mouse with impaired glycolysis, proline dehydrogenase activity may be de-repressed as was found to be the case in a lung cancer cell line along with increased expression after glucose deprivation (91). This shift would be unexpected given the preference of mammalian retinas for aspartate and glutamate as fuel sources under normal conditions (92). Indeed, proline abundance may be lower due to lower synthesis in the retinas of *RetΔGlut1* mice, since it relies on the availability of mitochondrial NADPH produced from NAD+ by NAD kinases, whose activity may be regulated by nutritional status (93).

Future studies will elucidate the distinct metabolic adaptations in photoreceptors and MGCs to glucose deprivation, and the impacts to the RPE when the normally high lactate efflux from the retina is substantially reduced.

Conclusion

In this study we demonstrated that GLUT1 is the primary glucose transporter in the outer retina, while GLUT3 predominates in the inner retina. When we deleted *Slc2a1* from all retinal neurons and MGC, we observed a selective impact on photoreceptors. In addition to rod cell death, rods and cones had impaired opsin synthesis and shorter OSs. Conditional deletion of *Slc2a1* from only rods also resulted in shorter rod OS. The two models presented here show that glucose uptake into rods is required for opsin synthesis, OS renewal, and viability. Cone survival is less dependent on GLUT1, indicating that cones rely less on glucose and glycolytic intermediates for viability and cell protection. Overall, our findings suggest that glucose deprivation compromises visual function not because of energy

deprivation but because of changes in the availability of building blocks required for outer segment renewal.

Supplementary Material

Refer to Web version on PubMed Central for supplementary material.

Acknowledgments

We would like to thank E. Dale Abel for providing the *GLUT1*$^{flox/flox}$ mice and Stephen Tsang for providing the *Pde6g-CreERT2* mice. We would also like to thank Benjamin Barnhart for his assistance with analysis of RNAseq libraries.

This work was supported by the National Institutes of Health R01EY026525 (NJP and KBB), R01EY12042 (NJP and NSP); R01EY031324 (JD), R01EY032462 (JD); T32AA007463 (JH) and P30EY025585 (Cleveland Clinic), the Department of Veterans Affairs I01BX002340, I01BX005844, and IK6BX005233 (ISS, and NSP), the Retina Research Foundation (JD), and an unrestricted award from Research to Prevent Blindness to Department of Ophthalmology of the Cleveland Clinic Lerner College of Medicine of Case Western Reserve University. The authors have no conflicts of interest in connection with this article.

References

1. Umino Y, Everhart D, Solessio E, Cusato K, Pan JC, Nguyen TH, Brown ET, Hafler R, Frio BA, Knox BE, Engbretson GA, Haeri M, Cui L, Glenn AS, Charron MJ, and Barlow RB (2006) Hypoglycemia leads to age-related loss of vision. Proc Natl Acad Sci U S A 103, 19541–19545 [PubMed: 17159157]
2. Ait-Ali N, Fridlich R, Millet-Puel G, Clerin E, Delalande F, Jaillard C, Blond F, Perrocheau L, Reichman S, Byrne LC, Olivier-Bandini A, Bellalou J, Moyse E, Bouillaud F, Nicol X, Dalkara D, van Dorsselaer A, Sahel JA, and Leveillard T (2015) Rod-derived cone viability factor promotes cone survival by stimulating aerobic glycolysis. Cell 161, 817–832 [PubMed: 25957687]
3. Wang W, Lee SJ, Scott PA, Lu X, Emery D, Liu Y, Ezashi T, Roberts MR, Ross JW, Kaplan HJ, and Dean DC (2016) Two-Step Reactivation of Dormant Cones in Retinitis Pigmentosa. Cell Rep 15, 372–385 [PubMed: 27050517]
4. Grenell A, Wang Y, Yam M, Swarup A, Dilan TL, Hauer A, Linton JD, Philp NJ, Gregor E, Zhu S, Shi Q, Murphy J, Guan T, Lohner D, Kolandaivelu S, Ramamurthy V, Goldberg AFX, Hurley JB, and Du J (2019) Loss of MPC1 reprograms retinal metabolism to impair visual function. Proc Natl Acad Sci U S A 116, 3530–3535 [PubMed: 30808746]
5. Wang W, Kini A, Wang Y, Liu T, Chen Y, Vukmanic E, Emery D, Liu Y, Lu X, Jin L, Lee SJ, Scott P, Liu X, Dean K, Lu Q, Fortuny E, James R, Kaplan HJ, Du J, and Dean DC (2019) Metabolic Deregulation of the Blood-Outer Retinal Barrier in Retinitis Pigmentosa. Cell Rep 28, 1323–1334 e1324 [PubMed: 31365873]
6. Petit L, Ma S, Cipi J, Cheng SY, Zieger M, Hay N, and Punzo C (2018) Aerobic Glycolysis Is Essential for Normal Rod Function and Controls Secondary Cone Death in Retinitis Pigmentosa. Cell Rep 23, 2629–2642 [PubMed: 29847794]
7. Swarup A, Samuels IS, Bell BA, Han JYS, Du J, Massenzio E, Abel ED, Boesze-Battaglia K, Peachey NS, and Philp NJ (2019) Modulating GLUT1 expression in retinal pigment epithelium decreases glucose levels in the retina: impact on photoreceptors and Muller glial cells. Am J Physiol Cell Physiol 316, C121–C133 [PubMed: 30462537]
8. Rajala A, Wang Y, Soni K, and Rajala RVS (2018) Pyruvate kinase M2 isoform deletion in cone photoreceptors results in age-related cone degeneration. Cell Death Dis 9, 737 [PubMed: 29970877]
9. Rajala A, Wang Y, Brush RS, Tsantilas K, Jankowski CSR, Lindsay KJ, Linton JD, Hurley JB, Anderson RE, and Rajala RVS (2018) Pyruvate kinase M2 regulates photoreceptor structure, function, and viability. Cell Death Dis 9, 240 [PubMed: 29445082]
10. Shen W, Lee SR, Mathai AE, Zhang R, Du J, Yam MX, Pye V, Barnett NL, Rayner CL, Zhu L, Hurley JB, Seth P, Hirabayashi Y, Furuya S, and Gillies MC (2021) Effect of selectively knocking

down key metabolic genes in Muller glia on photoreceptor health. Glia 69, 1966–1986 [PubMed: 33835598]

11. Weh E, Lutrzykowska Z, Smith A, Hager H, Pawar M, Wubben TJ, and Besirli CG (2020) Hexokinase 2 is dispensable for photoreceptor development but is required for survival during aging and outer retinal stress. Cell Death Dis 11, 422 [PubMed: 32499533]
12. Zhang R, Shen W, Du J, and Gillies MC (2020) Selective knockdown of hexokinase 2 in rods leads to age-related photoreceptor degeneration and retinal metabolic remodeling. Cell Death Dis 11, 885 [PubMed: 33082308]
13. Rajala A, Soni K, and Rajala RVS (2020) Metabolic and Non-metabolic Roles of Pyruvate Kinase M2 Isoform in Diabetic Retinopathy. Sci Rep 10, 7456 [PubMed: 32366925]
14. Han JYS, Kinoshita J, Bisetto S, Bell BA, Nowak RA, Peachey NS, and Philp NJ (2020) Role of monocarboxylate transporters in regulating metabolic homeostasis in the outer retina: Insight gained from cell-specific Bsg deletion. FASEB J 34, 5401–5419 [PubMed: 32112484]
15. Zhang Y, Zhang Y, Sun K, Meng Z, and Chen L (2019) The SLC transporter in nutrient and metabolic sensing, regulation, and drug development. J Mol Cell Biol 11, 1–13 [PubMed: 30239845]
16. Winkler BS, Starnes CA, Twardy BS, Brault D, and Taylor RC (2008) Nuclear magnetic resonance and biochemical measurements of glucose utilization in the cone-dominant ground squirrel retina. Invest Ophthalmol Vis Sci 49, 4613–4619 [PubMed: 18566456]
17. Winkler BS (1981) Glycolytic and oxidative metabolism in relation to retinal function. J Gen Physiol 77, 667–692 [PubMed: 6267165]
18. Ames A 3rd, and Li YY (1992) Energy requirements of glutamatergic pathways in rabbit retina. J Neurosci 12, 4234–4242 [PubMed: 1359032]
19. Wang L, Tornquist P, and Bill A (1997) Glucose metabolism in pig outer retina in light and darkness. Acta Physiol Scand 160, 75–81 [PubMed: 9179314]
20. Hurley JB (2021) Retina Metabolism and Metabolism in the Pigmented Epithelium: A Busy Intersection. Annu Rev Vis Sci 7, 665–692 [PubMed: 34102066]
21. Chinchore Y, Begaj T, Wu D, Drokhlyansky E, and Cepko CL (2017) Glycolytic reliance promotes anabolism in photoreceptors. Elife 6
22. Tran DH, and Wang ZV (2019) Glucose Metabolism in Cardiac Hypertrophy and Heart Failure. J Am Heart Assoc 8, e012673 [PubMed: 31185774]
23. Turco SJ, and Pickard JL (1982) Altered G-protein glycosylation in vesicular stomatitis virus-infected glucose-deprived baby hamster kidney cells. J Biol Chem 257, 8674–8679 [PubMed: 6284741]
24. Murray AR, Vuong L, Brobst D, Fliesler SJ, Peachey NS, Gorbatyuk MS, Naash MI, and Al-Ubaidi MR (2015) Glycosylation of rhodopsin is necessary for its stability and incorporation into photoreceptor outer segment discs. Hum Mol Genet 24, 2709–2723 [PubMed: 25637522]
25. Young CD, Lewis AS, Rudolph MC, Ruehle MD, Jackman MR, Yun UJ, Ilkun O, Pereira R, Abel ED, and Anderson SM (2011) Modulation of glucose transporter 1 (GLUT1) expression levels alters mouse mammary tumor cell growth in vitro and in vivo. PLoS One 6, e23205 [PubMed: 21826239]
26. Holoman NC, Aiello JJ, Trobenter TD, Tarchick MJ, Kozlowski MR, Makowski ER, De Vivo DC, Singh C, Sears JE, and Samuels IS (2021) Reduction of Glut1 in the Neural Retina But Not the RPE Alleviates Polyol Accumulation and Normalizes Early Characteristics of Diabetic Retinopathy. J Neurosci 41, 3275–3299 [PubMed: 33622781]
27. Koch SF, Tsai YT, Duong JK, Wu WH, Hsu CW, Wu WP, Bonet-Ponce L, Lin CS, and Tsang SH (2015) Halting progressive neurodegeneration in advanced retinitis pigmentosa. J Clin Invest 125, 3704–3713 [PubMed: 26301813]
28. Fadl BR, Brodie SA, Malasky M, Boland JF, Kelly MC, Kelley MW, Boger E, Fariss R, Swaroop A, and Campello L (2020) An optimized protocol for retina single-cell RNA sequencing. Mol Vis 26, 705–717 [PubMed: 33088174]
29. Stuart T, Butler A, Hoffman P, Hafemeister C, Papalexi E, Mauck WM 3rd, Hao Y, Stoeckius M, Smibert P, and Satija R (2019) Comprehensive Integration of Single-Cell Data. Cell 177, 1888–1902 e1821 [PubMed: 31178118]

30. Hao Y, Hao S, Andersen-Nissen E, Mauck WM 3rd, Zheng S, Butler A, Lee MJ, Wilk AJ, Darby C, Zager M, Hoffman P, Stoeckius M, Papalexi E, Mimitou EP, Jain J, Srivastava A, Stuart T, Fleming LM, Yeung B, Rogers AJ, McElrath JM, Blish CA, Gottardo R, Smibert P, and Satija R (2021) Integrated analysis of multimodal single-cell data. Cell 184, 3573–3587 e3529 [PubMed: 34062119]

31. Peng YR, Shekhar K, Yan W, Herrmann D, Sappington A, Bryman GS, van Zyl T, Do MTH, Regev A, and Sanes JR (2019) Molecular Classification and Comparative Taxonomics of Foveal and Peripheral Cells in Primate Retina. Cell 176, 1222–1237 e1222 [PubMed: 30712875]

32. Wagner E, McCaffery P, and Drager UC (2000) Retinoic acid in the formation of the dorsoventral retina and its central projections. Dev Biol 222, 460–470 [PubMed: 10837133]

33. Bell BA, Kaul C, and Hollyfield JG (2014) A protective eye shield for prevention of media opacities during small animal ocular imaging. Exp Eye Res 127, 280–287 [PubMed: 25245081]

34. Bell BA, Bonilha VL, Hagstrom SA, Anand-Apte B, Hollyfield JG, and Samuels IS (2019) Prolonged ocular exposure leads to retinal lesions in mice. Exp Eye Res 185, 107672 [PubMed: 31128100]

35. Schindelin J, Arganda-Carreras I, Frise E, Kaynig V, Longair M, Pietzsch T, Preibisch S, Rueden C, Saalfeld S, Schmid B, Tinevez JY, White DJ, Hartenstein V, Eliceiri K, Tomancak P, and Cardona A (2012) Fiji: an open-source platform for biological-image analysis. Nat Methods 9, 676–682 [PubMed: 22743772]

36. Yam M, Engel AL, Wang Y, Zhu S, Hauer A, Zhang R, Lohner D, Huang J, Dinterman M, Zhao C, Chao JR, and Du J (2019) Proline mediates metabolic communication between retinal pigment epithelial cells and the retina. J Biol Chem 294, 10278–10289 [PubMed: 31110046]

37. Pang Z, Chong J, Li S, and Xia J (2020) MetaboAnalystR 3.0: Toward an Optimized Workflow for Global Metabolomics. Metabolites 10

38. Shin BC, Cepeda C, Estrada-Sanchez AM, Levine MS, Hodaei L, Dai Y, Jung J, Ganguly A, Clark P, and Devaskar SU (2018) Neural Deletion of Glucose Transporter Isoform 3 Creates Distinct Postnatal and Adult Neurobehavioral Phenotypes. J Neurosci 38, 9579–9599 [PubMed: 30232223]

39. Watanabe T, Nagamatsu S, Matsushima S, Kirino T, and Uchimura H (1999) Colocalization of GLUT3 and choline acetyltransferase immunoreactivity in the rat retina. Biochem Biophys Res Commun 256, 505–511 [PubMed: 10080928]

40. Samson M, Emerson MM, and Cepko CL (2009) Robust marking of photoreceptor cells and pinealocytes with several reporters under control of the Crx gene. Dev Dyn 238, 3218–3225 [PubMed: 19882727]

41. Gospe SM 3rd, Baker SA, and Arshavsky VY (2010) Facilitative glucose transporter Glut1 is actively excluded from rod outer segments. J Cell Sci 123, 3639–3644 [PubMed: 20923839]

42. Kanow MA, Giarmarco MM, Jankowski CS, Tsantilas K, Engel AL, Du J, Linton JD, Farnsworth CC, Sloat SR, Rountree A, Sweet IR, Lindsay KJ, Parker ED, Brockerhoff SE, Sadilek M, Chao JR, and Hurley JB (2017) Biochemical adaptations of the retina and retinal pigment epithelium support a metabolic ecosystem in the vertebrate eye. Elife 6

43. He J, Yamamoto M, Sumiyama K, Konagaya Y, Terai K, Matsuda M, and Sato S (2021) Two-photon AMPK and ATP imaging reveals the bias between rods and cones in glycolysis utility. FASEB J 35, e21880 [PubMed: 34449091]

44. Daum JM, Keles Ö, Holwerda SJ, Kohler H, Rijli FM, Stadler M, and Roska B (2017) The formation of the light-sensing compartment of cone photoreceptors coincides with a transcriptional switch. Elife 6

45. Salinas RY, Pearring JN, Ding JD, Spencer WJ, Hao Y, and Arshavsky VY (2017) Photoreceptor discs form through peripherin-dependent suppression of ciliary ectosome release. J Cell Biol 216, 1489–1499 [PubMed: 28381413]

46. Obata S, and Usukura J (1992) Morphogenesis of the photoreceptor outer segment during postnatal development in the mouse (BALB/c) retina. Cell Tissue Res 269, 39–48 [PubMed: 1423483]

47. Lem J, Krasnoperova NV, Calvert PD, Kosaras B, Cameron DA, Nicolo M, Makino CL, and Sidman RL (1999) Morphological, physiological, and biochemical changes in rhodopsin knockout mice. Proc Natl Acad Sci U S A 96, 736–741 [PubMed: 9892703]

48. Humphries MM, Rancourt D, Farrar GJ, Kenna P, Hazel M, Bush RA, Sieving PA, Sheils DM, McNally N, Creighton P, Erven A, Boros A, Gulya K, Capecchi MR, and Humphries P (1997) Retinopathy induced in mice by targeted disruption of the rhodopsin gene. Nat Genet 15, 216–219 [PubMed: 9020854]
49. Daniele LL, Insinna C, Chance R, Wang J, Nikonov SS, and Pugh EN Jr. (2011) A mouse M-opsin monochromat: retinal cone photoreceptors have increased M-opsin expression when S-opsin is knocked out. Vision Res 51, 447–458 [PubMed: 21219924]
50. Viegas FO, and Neuhauss SCF (2021) A Metabolic Landscape for Maintaining Retina Integrity and Function. Front Mol Neurosci 14, 656000 [PubMed: 33935647]
51. Carter-Dawson L, Alvarez RA, Fong SL, Liou GI, Sperling HG, and Bridges CD (1986) Rhodopsin, 11-cis vitamin A, and interstitial retinol-binding protein (IRBP) during retinal development in normal and rd mutant mice. Dev Biol 116, 431–438 [PubMed: 3732615]
52. Duncan JL, LaVail MM, Yasumura D, Matthes MT, Yang H, Trautmann N, Chappelow AV, Feng W, Earp HS, Matsushima GK, and Vollrath D (2003) An RCS-like retinal dystrophy phenotype in mer knockout mice. Invest Ophthalmol Vis Sci 44, 826–838 [PubMed: 12556419]
53. Nandrot EF, Kim Y, Brodie SE, Huang X, Sheppard D, and Finnemann SC (2004) Loss of synchronized retinal phagocytosis and age-related blindness in mice lacking alphavbeta5 integrin. J Exp Med 200, 1539–1545 [PubMed: 15596525]
54. Yu C, Roubeix C, Sennlaub F, and Saban DR (2020) Microglia versus Monocytes: Distinct Roles in Degenerative Diseases of the Retina. Trends Neurosci 43, 433–449 [PubMed: 32459994]
55. Guo M, Schwartz TD, Dunaief JL, and Cui QN (2021) Myeloid cells in retinal and brain degeneration. FEBS J
56. Flynn E, Ueda K, Auran E, Sullivan JM, and Sparrow JR (2014) Fundus autofluorescence and photoreceptor cell rosettes in mouse models. Invest Ophthalmol Vis Sci 55, 5643–5652 [PubMed: 25015357]
57. Bell BA, Kaul C, Bonilha VL, Rayborn ME, Shadrach K, and Hollyfield JG (2015) The BALB/c mouse: Effect of standard vivarium lighting on retinal pathology during aging. Exp Eye Res 135, 192–205 [PubMed: 25895728]
58. Sanz MM, Johnson LE, Ahuja S, Ekstrom PA, Romero J, and van Veen T (2007) Significant photoreceptor rescue by treatment with a combination of antioxidants in an animal model for retinal degeneration. Neuroscience 145, 1120–1129 [PubMed: 17293057]
59. Trachsel-Moncho L, Benlloch-Navarro S, Fernández-Carbonell Á, Ramírez-Lamelas DT, Olivar T, Silvestre D, Poch E, and Miranda M (2018) Oxidative stress and autophagy-related changes during retinal degeneration and development. Cell Death Dis 9, 812 [PubMed: 30042417]
60. Du J, Cleghorn W, Contreras L, Linton JD, Chan GC, Chertov AO, Saheki T, Govindaraju V, Sadilek M, Satrustegui J, and Hurley JB (2013) Cytosolic reducing power preserves glutamate in retina. Proc Natl Acad Sci U S A 110, 18501–18506 [PubMed: 24127593]
61. Hurley JB, Lindsay KJ, and Du J (2015) Glucose, lactate, and shuttling of metabolites in vertebrate retinas. J Neurosci Res 93, 1079–1092 [PubMed: 25801286]
62. Du J, Rountree A, Cleghorn WM, Contreras L, Lindsay KJ, Sadilek M, Gu H, Djukovic D, Raftery D, Satrustegui J, Kanow M, Chan L, Tsang SH, Sweet IR, and Hurley JB (2016) Phototransduction Influences Metabolic Flux and Nucleotide Metabolism in Mouse Retina. J Biol Chem 291, 4698–4710 [PubMed: 26677218]
63. Poitry-Yamate CL, Poitry S, and Tsacopoulos M (1995) Lactate released by Müller glial cells is metabolized by photoreceptors from mammalian retina. J Neurosci 15, 5179–5191 [PubMed: 7623144]
64. Winkler BS, Arnold MJ, Brassell MA, and Puro DG (2000) Energy metabolism in human retinal Müller cells. Invest Ophthalmol Vis Sci 41, 3183–3190 [PubMed: 10967082]
65. Gould GW, Thomas HM, Jess TJ, and Bell GI (1991) Expression of human glucose transporters in Xenopus oocytes: kinetic characterization and substrate specificities of the erythrocyte, liver, and brain isoforms. Biochemistry 30, 5139–5145 [PubMed: 2036379]
66. Furukawa T, Morrow EM, and Cepko CL (1997) Crx, a novel otx-like homeobox gene, shows photoreceptor-specific expression and regulates photoreceptor differentiation. Cell 91, 531–541 [PubMed: 9390562]

67. Montana CL, Lawrence KA, Williams NL, Tran NM, Peng GH, Chen S, and Corbo JC (2011) Transcriptional regulation of neural retina leucine zipper (Nrl), a photoreceptor cell fate determinant. J Biol Chem 286, 36921–36931 [PubMed: 21865162]

68. Nishida A, Furukawa A, Koike C, Tano Y, Aizawa S, Matsuo I, and Furukawa T (2003) Otx2 homeobox gene controls retinal photoreceptor cell fate and pineal gland development. Nat Neurosci 6, 1255–1263 [PubMed: 14625556]

69. Okawa H, Sampath AP, Laughlin SB, and Fain GL (2008) ATP consumption by mammalian rod photoreceptors in darkness and in light. Curr Biol 18, 1917–1921 [PubMed: 19084410]

70. Bakall B, Marmorstein LY, Hoppe G, Peachey NS, Wadelius C, and Marmorstein AD (2003) Expression and localization of bestrophin during normal mouse development. Invest Ophthalmol Vis Sci 44, 3622–3628 [PubMed: 12882816]

71. Bonezzi PJ, Stabio ME, and Renna JM (2018) The Development of Mid-Wavelength Photoresponsivity in the Mouse Retina. Curr Eye Res 43, 666–673 [PubMed: 29447486]

72. Cunnane SC, Trushina E, Morland C, Prigione A, Casadesus G, Andrews ZB, Beal MF, Bergersen LH, Brinton RD, de la Monte S, Eckert A, Harvey J, Jeggo R, Jhamandas JH, Kann O, la Cour CM, Martin WF, Mithieux G, Moreira PI, Murphy MP, Nave KA, Nuriel T, Oliet SHR, Saudou F, Mattson MP, Swerdlow RH, and Millan MJ (2020) Brain energy rescue: an emerging therapeutic concept for neurodegenerative disorders of ageing. Nat Rev Drug Discov 19, 609–633 [PubMed: 32709961]

73. Palfi A, Millington-Ward S, Chadderton N, O'Reilly M, Goldmann T, Humphries MM, Li T, Wolfrum U, Humphries P, Kenna PF, and Farrar GJ (2010) Adeno-associated virus-mediated rhodopsin replacement provides therapeutic benefit in mice with a targeted disruption of the rhodopsin gene. Hum Gene Ther 21, 311–323 [PubMed: 19824806]

74. Sakurai K, Onishi A, Imai H, Chisaka O, Ueda Y, Usukura J, Nakatani K, and Shichida Y (2007) Physiological properties of rod photoreceptor cells in green-sensitive cone pigment knock-in mice. J Gen Physiol 130, 21–40 [PubMed: 17591985]

75. Shi G, Yau KW, Chen J, and Kefalov VJ (2007) Signaling properties of a short-wave cone visual pigment and its role in phototransduction. J Neurosci 27, 10084–10093 [PubMed: 17881515]

76. Otteson DC, Liu Y, Lai H, Wang C, Gray S, Jain MK, and Zack DJ (2004) Kruppel-like factor 15, a zinc-finger transcriptional regulator, represses the rhodopsin and interphotoreceptor retinoid-binding protein promoters. Invest Ophthalmol Vis Sci 45, 2522–2530 [PubMed: 15277472]

77. Botta S, de Prisco N, Marrocco E, Renda M, Sofia M, Curion F, Bacci ML, Ventrella D, Wilson C, Gesualdo C, Rossi S, Simonelli F, and Surace EM (2017) Targeting and silencing of rhodopsin by ectopic expression of the transcription factor KLF15. JCI Insight 2

78. Yamamoto J, Ikeda Y, Iguchi H, Fujino T, Tanaka T, Asaba H, Iwasaki S, Ioka RX, Kaneko IW, Magoori K, Takahashi S, Mori T, Sakaue H, Kodama T, Yanagisawa M, Yamamoto TT, Ito S, and Sakai J (2004) A Kruppel-like factor KLF15 contributes fasting-induced transcriptional activation of mitochondrial acetyl-CoA synthetase gene AceCS2. J Biol Chem 279, 16954–16962 [PubMed: 14960588]

79. Hsieh PN, Fan L, Sweet DR, and Jain MK (2019) The Kruppel-Like Factors and Control of Energy Homeostasis. Endocr Rev 40, 137–152 [PubMed: 30307551]

80. Gray S, Feinberg MW, Hull S, Kuo CT, Watanabe M, Sen-Banerjee S, DePina A, Haspel R, and Jain MK (2002) The Kruppel-like factor KLF15 regulates the insulin-sensitive glucose transporter GLUT4. J Biol Chem 277, 34322–34328 [PubMed: 12097321]

81. Punzo C, Kornacker K, and Cepko CL (2009) Stimulation of the insulin/mTOR pathway delays cone death in a mouse model of retinitis pigmentosa. Nat Neurosci 12, 44–52 [PubMed: 19060896]

82. Xue Y, Wang SK, Rana P, West ER, Hong CM, Feng H, Wu DM, and Cepko CL (2021) AAV-Txnip prolongs cone survival and vision in mouse models of retinitis pigmentosa. Elife 10

83. Wang L, Pavlou S, Du X, Bhuckory M, Xu H, and Chen M (2019) Glucose transporter 1 critically controls microglial activation through facilitating glycolysis. Mol Neurodegener 14, 2 [PubMed: 30634998]

84. Joyal JS, Sun Y, Gantner ML, Shao Z, Evans LP, Saba N, Fredrick T, Burnim S, Kim JS, Patel G, Juan AM, Hurst CG, Hatton CJ, Cui Z, Pierce KA, Bherer P, Aguilar E, Powner MB, Vevis

K, Boisvert M, Fu Z, Levy E, Fruttiger M, Packard A, Rezende FA, Maranda B, Sapieha P, Chen J, Friedlander M, Clish CB, and Smith LE (2016) Retinal lipid and glucose metabolism dictates angiogenesis through the lipid sensor Ffar1. Nat Med 22, 439–445 [PubMed: 26974308]

85. Elhassan YS, Kluckova K, Fletcher RS, Schmidt MS, Garten A, Doig CL, Cartwright DM, Oakey L, Burley CV, Jenkinson N, Wilson M, Lucas SJE, Akerman I, Seabright A, Lai YC, Tennant DA, Nightingale P, Wallis GA, Manolopoulos KN, Brenner C, Philp A, and Lavery GG (2019) Nicotinamide Riboside Augments the Aged Human Skeletal Muscle NAD(+) Metabolome and Induces Transcriptomic and Anti-inflammatory Signatures. Cell Rep 28, 1717–1728 e1716 [PubMed: 31412242]
86. Mehmel M, Jovanovic N, and Spitz U (2020) Nicotinamide Riboside-The Current State of Research and Therapeutic Uses. Nutrients 12
87. Newgard CB, An J, Bain JR, Muehlbauer MJ, Stevens RD, Lien LF, Haqq AM, Shah SH, Arlotto M, Slentz CA, Rochon J, Gallup D, Ilkayeva O, Wenner BR, Yancy WS Jr., Eisenson H, Musante G, Surwit RS, Millington DS, Butler MD, and Svetkey LP (2009) A branched-chain amino acid-related metabolic signature that differentiates obese and lean humans and contributes to insulin resistance. Cell Metab 9, 311–326 [PubMed: 19356713]
88. McCann MR, George De la Rosa MV, Rosania GR, and Stringer KA (2021) L-Carnitine and Acylcarnitines: Mitochondrial Biomarkers for Precision Medicine. Metabolites 11
89. Kowaloff EM, Phang JM, Granger AS, and Downing SJ (1977) Regulation of proline oxidase activity by lactate. Proc Natl Acad Sci U S A 74, 5368–5371 [PubMed: 271958]
90. Hancock CN, Liu W, Alvord WG, and Phang JM (2016) Co-regulation of mitochondrial respiration by proline dehydrogenase/oxidase and succinate. Amino Acids 48, 859–872 [PubMed: 26660760]
91. Pandhare J, Donald SP, Cooper SK, and Phang JM (2009) Regulation and function of proline oxidase under nutrient stress. J Cell Biochem 107, 759–768 [PubMed: 19415679]
92. Li B, Zhang T, Liu W, Wang Y, Xu R, Zeng S, Zhang R, Zhu S, Gillies MC, Zhu L, and Du J (2020) Metabolic Features of Mouse and Human Retinas: Rods versus Cones, Macula versus Periphery, Retina versus RPE. iScience 23, 101672 [PubMed: 33196018]
93. Hoxhaj G, Ben-Sahra I, Lockwood SE, Timson RC, Byles V, Henning GT, Gao P, Selfors LM, Asara JM, and Manning BD (2019) Direct stimulation of NADP(+) synthesis through Akt-mediated phosphorylation of NAD kinase. Science 363, 1088–1092 [PubMed: 30846598]

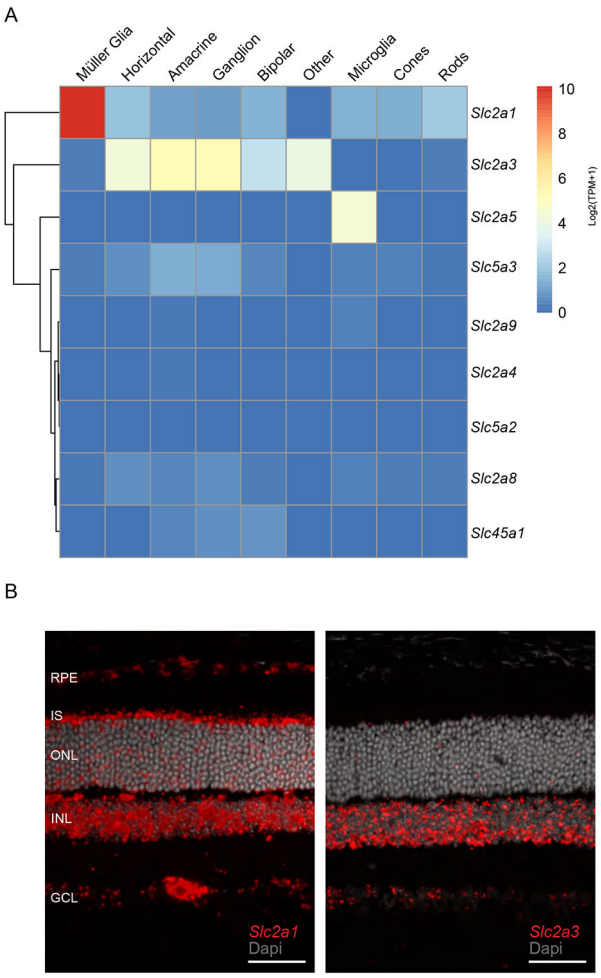

FIGURE 1. GLUT1 is the primary glucose transporter in the outer retina

A) scRNAseq analysis of genes encoding solute transporters with glucose transport activity (GO:5355) from 1-month-old murine retina (GSE153674). Each cell type shows the Log 2 transformed average transcript per million (TPM).

B) Expression of *Slc2a1* and *Slc2a3* in control mouse retinas using in situ hybridization. Left panel shows *Slc2a1* transcript, right panel shows *Slc2a3* transcript detected (red) (Scale bar indicates 50 μm).

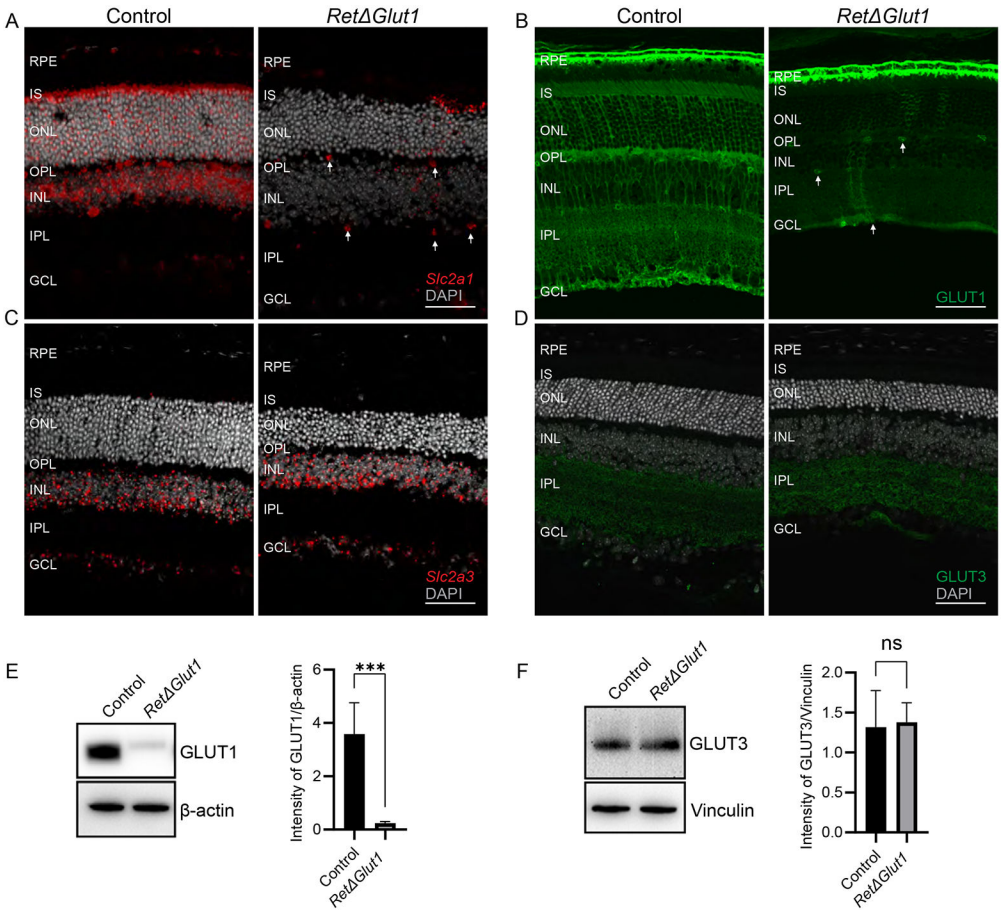

FIGURE 2. Deletion of GLUT1 from the retina does not result in compensatory changes in expression of GLUT3

A) *In situ* hybridization to detect the localization of *Slc2a1*. The *RetΔGlut1* mice had a loss of *Slc2a1* (red) signal in the inner and outer retina with intermittent expression. *Slc2a1* expression seen in inner retinal blood vessels (as indicated by white arrows) and the RPE (Scale bar indicates 50 μm).

B) Immunostaining of GLUT1 (green) in control and *RetΔGlut1* mice. White arrows indicate GLUT1 expression in inner retinal blood vessels. (Scale bar indicates 50 μm).

C) *In situ* hybridization of *Slc2a3* from control and *RetΔGlut1* mice at 1-month of age. (Scale bar indicates 50 μm).

D) Immunostaining of GLUT3 (green) in control and *RetΔGlut1* mice at 1-month of age. (Scale bar indicates 50 μm).

E) Western blot analysis of GLUT1 expression in control and *RetΔGlut1* retinas. 5 μg retina protein was loaded per well. Blots are representative of N=5. Bars indicate average ± SD of GLUT1 intensity normalized to β-actin for N = 5 mice.

F) Western blot analysis of GLUT3 expression in control and *RetΔGlut1* retinas. 5 μg retina protein was loaded per well. Blots are representative of N=3. Bars indicate average ± SD of GLUT3 intensity normalized to Vinculin for N = 3 mice.

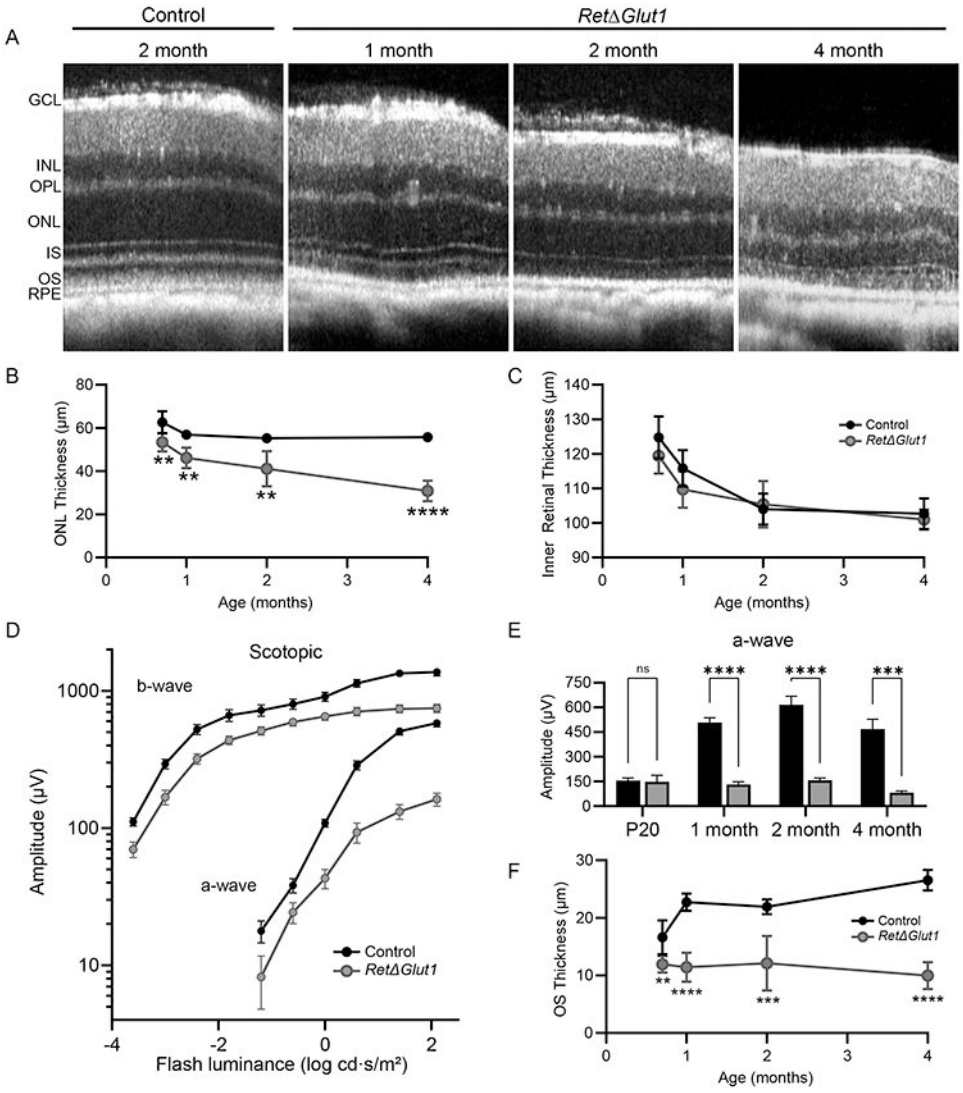

FIGURE 3. Rods degenerate in mice lacking retinal GLUT1 expression

A) Averaged SD-OCT B-scan from the horizontal meridian of retinas from 2-month-old control and 1, 2, and 4-month-old *RetΔGlut1* mice. GCL, INL, OPL, ONL, IS, OS and RPE are indicated.

B) ONL layer thickness measured from volumetric SD-OCT scans at P20, 1 month, 2 months, and 4 months of age. Data points indicate average (± SD) for 3-6 mice.

C) Inner Retinal Thickness (OPL-GCL) measured from volumetric SD-OCT scans at P20, 1 month, 2 months, and 4 months of age. Data points indicate average (± SD) for 3-6 mice.

D) Luminance-response functions for a-waves and b-waves recorded from 1-month mice. Data points indicate average (± SEM) for 13-14 mice.

E) Maximum amplitudes for a-waves (at 1.4 log cd · s/m^2 luminance) at the ages indicated. Bars indicate average (± SEM) for 8-14 mice.

F) OS length measured from volumetric SD-OCT scans at P20, 1-, 2- and 4-months of age. Data points indicate average (± SD) for 3-6 mice.

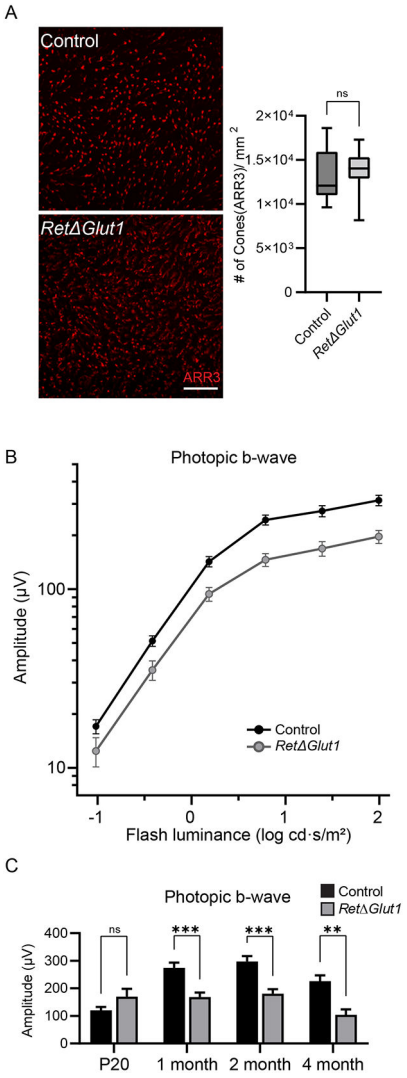

FIGURE 4. Cones of *RetΔGlut1* mice have impaired function but do not degenerate

A) Fluorescence images of retinal flat mounts immunolabeled for cone arrestin ARR3 (red). Scale bar indicates 100 μm. Box plots of estimations of cone density per mm^2 at various radial positions halfway between optic nerve and edge of the retina in flattened retinas for 3 mice.

B) Luminance response functions from photopic ERG b-waves recorded from 1-month control and *RetΔGlut1* mice under light-adapted conditions. Data points indicate average (± SEM) for 13-14 mice.

C) Maximum amplitudes for photopic b-waves (for flashes at 1.4 log cd · s/m^2 luminance) for mice at the ages indicated. Bars indicate average (± SEM) for 8-14 mice.

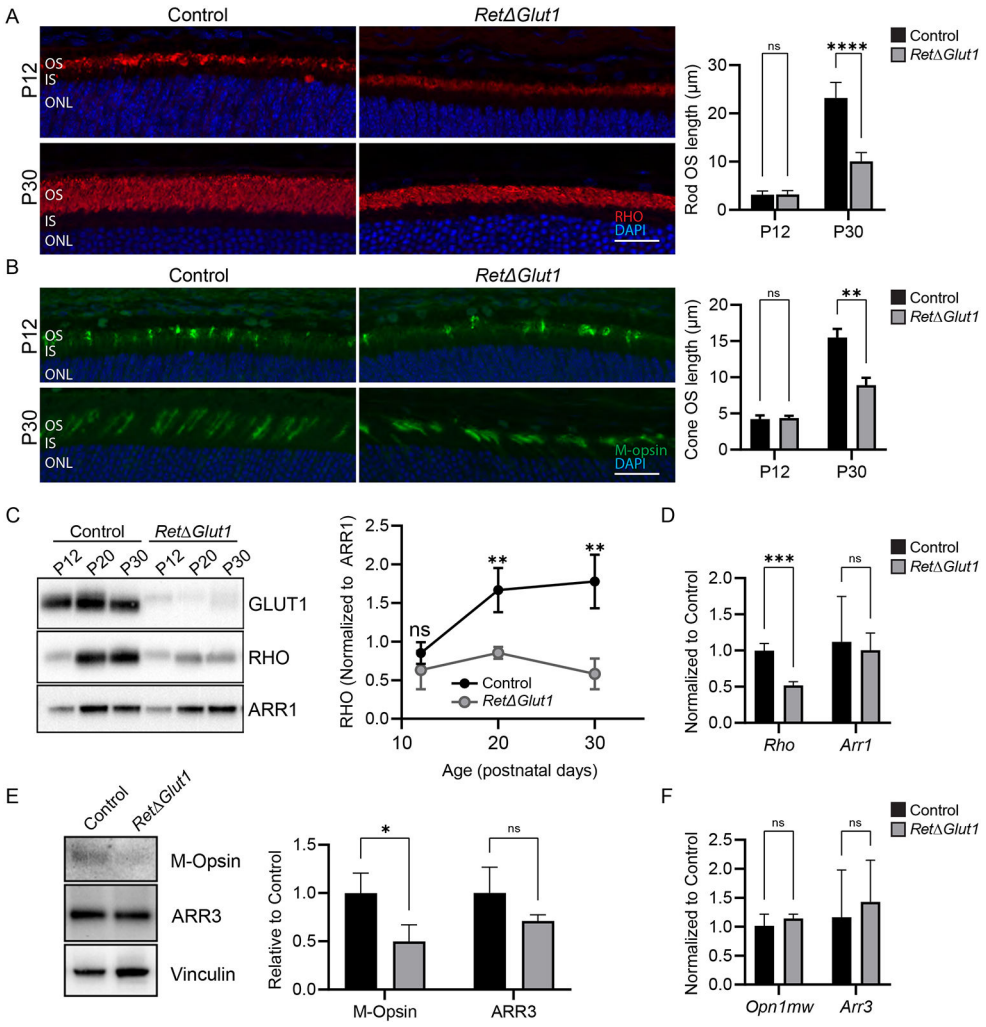

FIGURE 5. Reduced opsin synthesis contributes to the impaired renewal of rod and cone OS

A) Left: Retina cryosections from control and *RetΔGlut1* mice immunolabeled for RHO (red) and counterstained with DAPI (blue) at P12 (top row) and P30 (bottom row). OS lengths were estimated with ImageJ from images of cryosections like those shown from P12 and 1-month control and *RetΔGlut1* mice. Right: Bars indicate average ± SD for 3 mice. Scale bar indicates 50 μm.

B) Left: Retina cryosections from control and *RetΔGlut1* mice immunolabeled for cone opsin (green) and counterstained with DAPI (blue) at P12 (top row) and P30 (bottom row). OS lengths were estimated with ImageJ from images like those shown at left, from P12 and 1-month control and *RetΔGlut1* mice. Right: Bars indicate average ± SD for 3 mice. Scale bar indicates 50 μm.

C) Western blots showing relative GLUT1 (5 μg/well), Rhodopsin (RHO) (0.25 μg/well) and rod arrestin (ARR1) (0.25 μg/well) levels in retina lysates from control and *RetΔGlut1* mice aged P12, P20 and P30. The ratio of density signals for rhodopsin relative to ARR1 at various ages was estimated from retinas of control and *RetΔGlut1* mice. Data points indicate average ± SD for 3 mice.

D) Relative transcription levels for rhodopsin (*Rho*) and rod arrestin (*Arr1*) estimated from real-time RT-PCR analysis with probes for mouse, *rho* and *Arr1* for retinas of P30 control and *RetΔGlut1* mice. Bars indicate average ± SD for 3 mice

E) Left: Western blots showing relative M-opsin and cone arrestin (ARR3) levels in retina lysates (2.5 μg/well) from control and *RetΔGlut1* mice aged P30. Right: Ratio of density signals for M-opsin and ARR3 relative to vinculin at P30 estimated from retinas of control and *RetΔGlut1* mice. Bars indicate average ± SD for 3 mice

F) Relative transcription levels for M-opsin and cone arrestin estimated from real-time RT-PCR analysis with probes for mouse *Opn1mw* and (*Arr3)* for retinas of P30 control and *RetΔGlut1* mice. Bars indicate average ± SD for 3 mice.

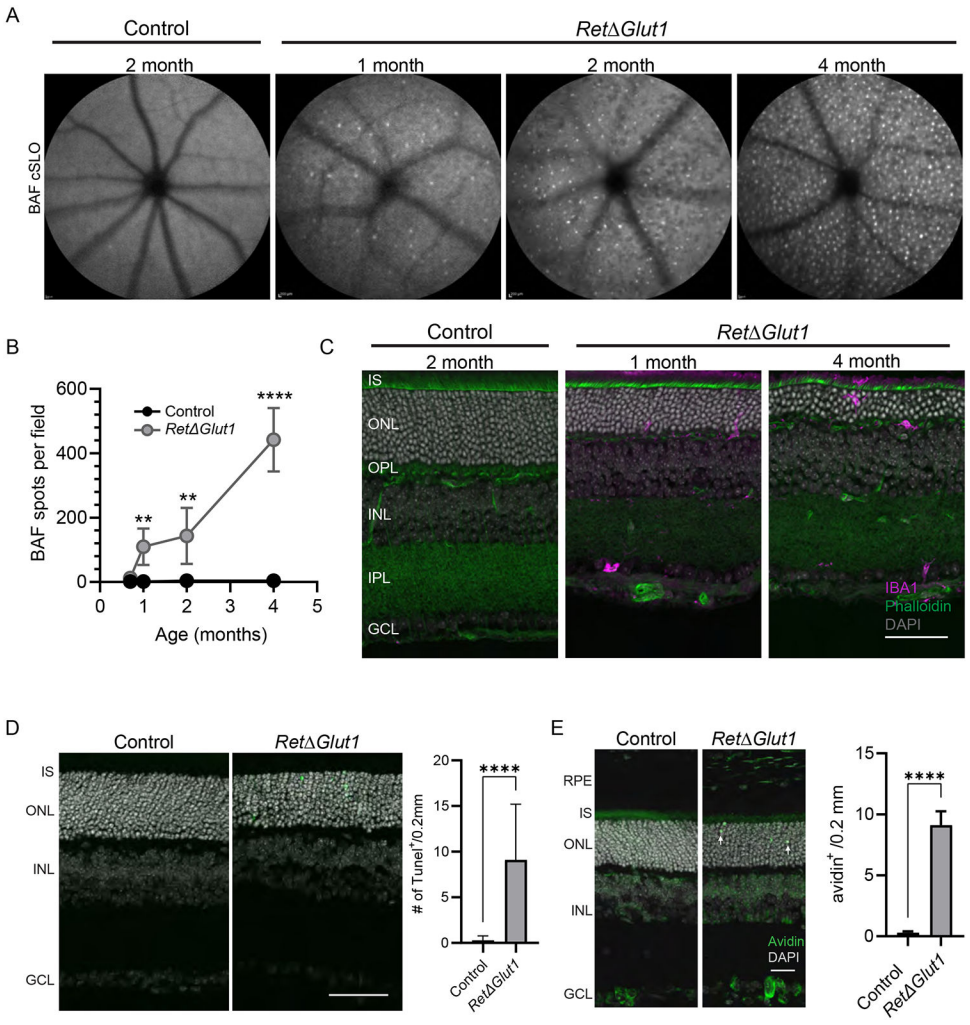

FIGURE 6. Increased inflammation in the outer retina of *RetΔGlut1* mice

A) Representative 55° wide-field BAF-cSLO images obtained from 2-month control and 1-, 2- and 4-month *RetΔGlut1* mice.

B) Number of BAF-cSLO identified hyperfluorescent foci were quantified at each age in *RetΔGlut1* and control mice. Data points indicate average ± SD for 3-6 mice.

C) Iba-1 immunofluorescence (magenta) in retina cryosections from control, 2 month and 4-month *RetΔGlut1* mice counterstained with Phalloidin (green) DAPI (gray). Scale bar indicates 50 μm. IS, inner segments; ONL, outer nuclear layer; OPL, outer plexiform layer, INL, inner nuclear layer; IPL, inner plexiform layer, GCL, ganglion cell layer

D) Left: TUNEL labeling (green) of retina cryosections from P15 control and *RetΔGlut1* mice, counterstained with DAPI (gray). Scale bar indicates 50 μm. Right: quantification of TUNEL per 0.2 mm length retina from immunofluorescent images. Bars indicate average ± SD for 2 mice.

E) Left: Avidin labeling (green) of retina cryosections from control and *RetΔGlut1* at P15 with DAPI counterstain (gray). Scale bar indicates 25 μm. Right: Quantification of avidin positive cells in oriented fluorescence images within 0.2 mm wide field of view. Bars

indicate average ± SD for 3 mice. RPE, retinal pigmented epithelium; IS, inner segments; ONL, outer nuclear layer; INL, inner nuclear layer; GCL, ganglion cell layer.

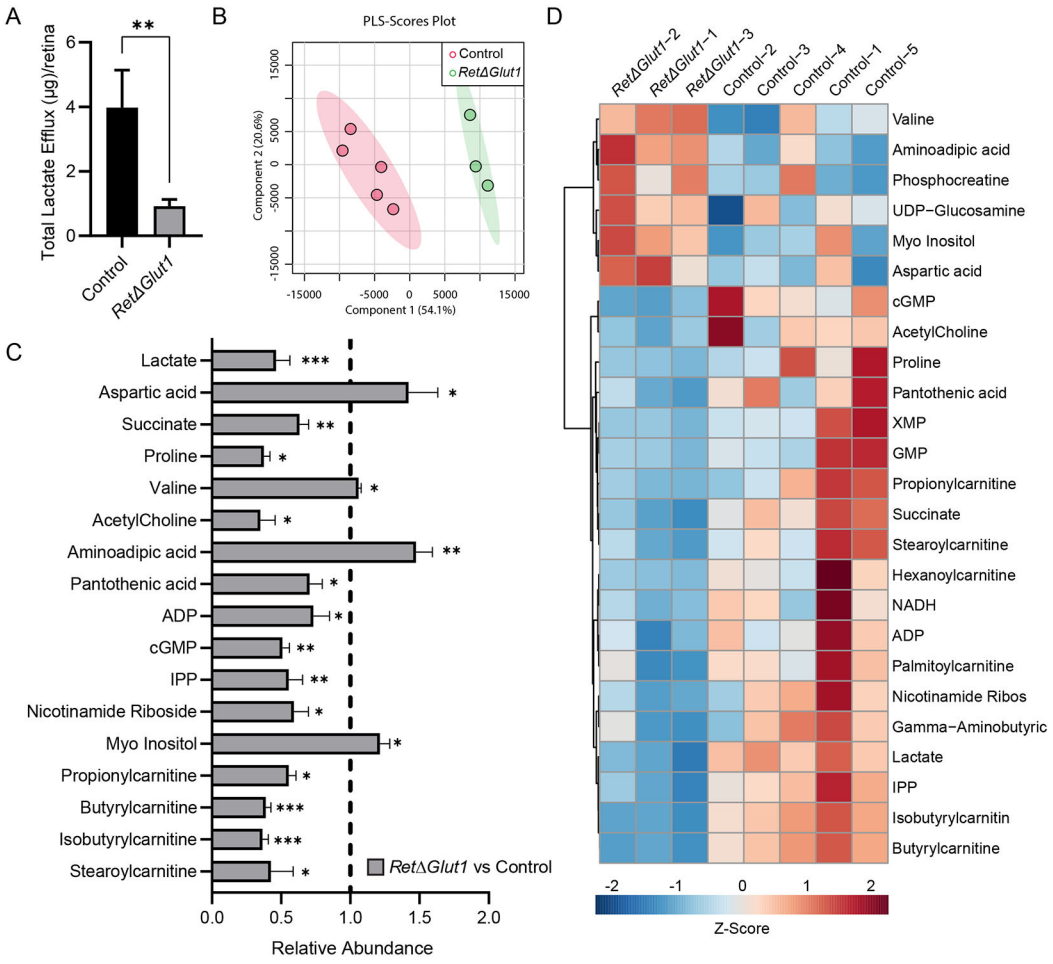

FIGURE 7. *RetΔGlut1* mice have reduced lactate efflux and an altered metabolic profile

A) Lactate efflux from isolated retinas incubated for 1 one hour in Ringer's with 5mM glucose from control and *RetΔGlut1* mice. Bars indicate average ± SEM for 4 retinas.

B) Partial Least-Squares Discriminant Analysis (PLS-DA) of Control and *RetΔGlut1* samples from LC-MS data. Data points indicate results from 5 control and 3 *RetΔGlut1.*

C) Metabolomics analysis of significant metabolites changed in *RetΔGlut1* retina samples. Raw data were normalized to the control average (hashed line), and statistical significance was obtained from T-tests after Pareto scaling. Bars indicate average (± SD) for 3-5 mice

D) Heat map of top 25 metabolites changed based on statistical significance or fold change between control and *RetΔGlut1* retina samples, after Pareto scaling.

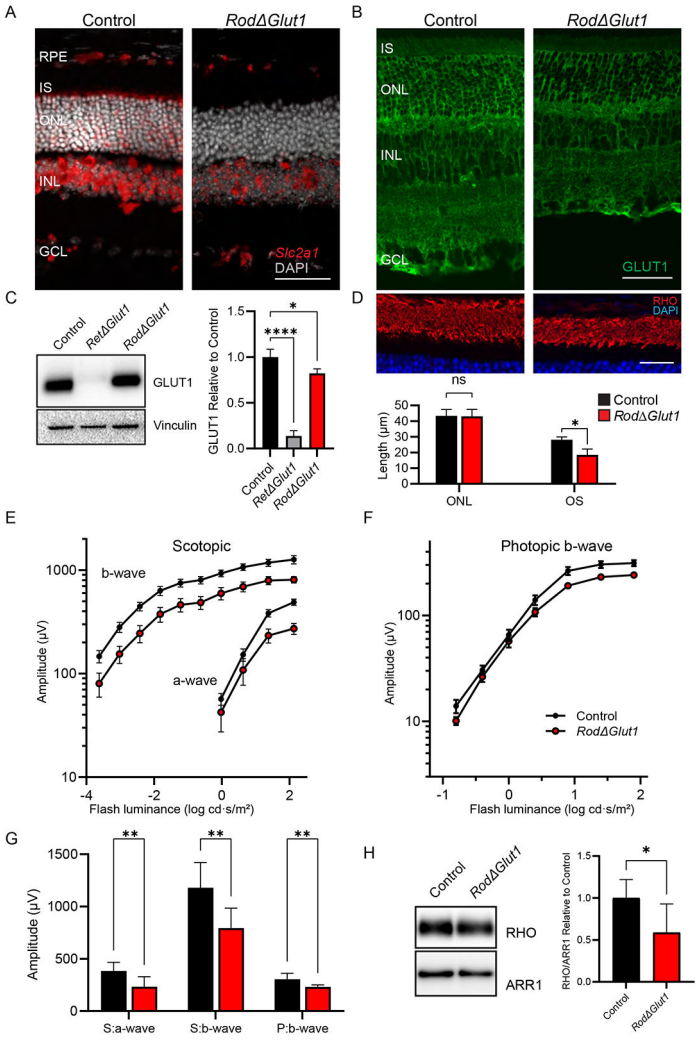

FIGURE 8. Loss of GLUT1 from rods results in impaired OS turnover and reduced ERG amplitude, but impacts are less severe than in *RetΔGlut1*

A) *In situ* hybridization for *Slc2a1* transcripts (red) in control and *RodΔGlut1*. Scale bar indicates 50 μm.

B) Immunofluorescence for GLUT1 (green) in control and *RodΔGlut1* retinas. Scale bar indicates 50 μm.

C) Western blot analysis of GLUT1 expression in control, *RetΔGlut1*, and *RodΔGlut1* retinas (5 μg /well). Blots are representative of N=3 mice. Quantification of relative expression of GLUT1 in retinas of control, *RetΔGlut1*, and *RodΔGlut1*. The intensity of GLUT1 was normalized to Vinculin. Bars indicate average (± SD) for 3 mice.

D) Retina cryosections from control and *RodΔGlut1* mice 1-month post-tamoxifen injection immunolabeled for RHO (red) and counterstained with DAPI (blue). Scale bar indicates 25 μm. ONL thickness and OS lengths were estimated with ImageJ. Bars indicate average (± SD) for 3 mice.

E) Luminance response plots from peak amplitudes of scotopic a-waves and b-waves recorded from control and *RodΔGlut1* mice 1-month post-tamoxifen injection. Data points indicate average (± SEM) for 7 mice

F) Luminance response plots from photopic b-waves of control and *RodΔGlut1* mice 1-month post-tamoxifen injection. Data points indicate average (± SEM) for 7 mice
G) Maximum amplitudes for scotopic a- and b- waves (S:a-wave, and S:b-wave) and photopic b-wave (P:b-wave) at 1.4 log cd · s/m^2 luminance. Bars indicate average (± SD) for 7 mice.
H) Left: Western blot analysis of expression of RHO (0.25 μg/well), and ARR1 (0.25 μg/well) in control and *RodΔGlut1* mice 1-month post-tamoxifen injection. Right: Bars indicate average (± SD) for 5-7 mice.

Table 1.

Antibodies used in this study.

Antigen	Supplier	Product no.	Species	Dilution (WB)	Dilution (IF)
GLUT1	Alpha Diagnostics	GT11-A	rabbit	1:2000	1:250
GLUT3	Alpha Diagnostics	GT31-A	rabbit	1:1000	1:100
Rhodopsin	Santa Cruz	sc-57432 (1D4)	mouse	1:1000	1:250
Rod arrestin (Arr1)	Philp Lab		rabbit	1:1000	not used
M-opsin	Millipore	ab5405	rabbit	1:1000	1:200
cone arrestin (Arr3)	EMD/Millipore	ab15282	rabbit	1:1000	1:1000
Iba-1	Waco	19-19741	rabbit	not used	1:100
Vinculin	Cell Signaling	13901	rabbit	1:1000	not used
β-actin	Cell Signaling	4970	rabbit	1:2000	not used
anti-mouse IgG- 488	Invitrogen	A32766	donkey	not used	1:500
anti-mouse IgG- 555	Invitrogen	A32773	donkey	not used	1:500
anti-rabbit IgG- 488	Invitrogen	A32790	donkey	not used	1:500
anti-rabbit IgG- 555	Invitrogen	A32794	donkey	not used	1:500
anti-rabbit IgG-HRP	Jackson Immuno Research	111-035-144	goat	1:2000	not used
anti-mouse IgG-HRP	Jackson Immuno Research	115-035-062	goat	1:2000	not used

Table 2.

Primers used in this study.

Primers for qPCR		
	Forward (5′–3′)	**Reverse (5′–3′)**
Rplp0	AGATTCGGGATATGCTGTTGGC	TCGGGTCCTAGACCAGTGTTC
Rho	CCACCACCCTCTACACATCAC	ACCACAGGGCGATTTCACC
Opn1mw	TCTATGGCTACTTCGTTCTGGG	GCCTGTGATTCCACACAATGA
Arrestin 1 (Arr1)	GGTCAGGGTGACATACACCTT	GCCTGCGGGAAGACCAATAAA
Arrestin 3 (Arr3)	GAGCCCATTGATGGAGTCGT	GGGCAGGTTAGCAACCATCT
Primers for genotyping		
GLUT1 flox	CTGTGAGTTCCTGAGACCCTG	CCCAGGCAAGGAAGTAGTTC
Cre	CCATCTGCCACCAGCCAG	TCGCCATCTTCCAGCAGG
Pde6g $^{tm1(CRE/ERT2)}$	GGTCAGATTCCAGTGTGTGGG	CTTAGGTGGTCCTTTCCTGGG GTTTAGCTGGCCCAAATGTTG